

# MECHANICAL PROPERTIES OF 2D FLEXYNE AND REFLEXYNE POLYPHENYLACETYLENE NETWORKS: A COMPARATIVE COMPUTER STUDIES WITH VARIOUS FORCE-FIELDS

LARA TRAPANI, RUBEN GATT, LUKE MIZZI  
AND JOSEPH N. GRIMA

*Metamaterials Unit, Faculty of Science, University of Malta  
Msida MSD 2080, Malta*

(received: 29 April 2015; revised: 18 May 2015;  
accepted: 22 June 2015; published online: 6 July 2015)

**Abstract:** Auxetic materials exhibit the very unusual property of becoming wider when stretched and narrower when compressed, – they have a negative Poisson’s ratio. This unusual behaviour is the source of many desired effects in the materials’ properties and it is therefore, no wonder that auxetics are described as being superior to conventional materials in many practical applications. Here we make use of force-field based molecular modelling simulations in order to investigate the mechanical properties of polypheyleacetylene systems known as  $(n, m)$ -flexyne and  $(n, m)$ -reflexyne in an attempt to extend the existing knowledge there is regarding these systems. These systems have already attracted considerable consideration since negative on-axis Poisson’s ratios have been discovered for the reflexynes.

We first developed a methodology for the modelling and property determination of flexyne and reflexyne network systems which we validated against existing published data. Then, extended the study to prove the simulated results were independent of the modelling methodology or the force-field used. In particular, we showed that on-axis auxeticity in the reflexynes is a force-field independent property, *i.e.* a property which is not an artefact of the simulations but a property which is likely to be present in the real materials if these were to be synthesised.

We also studied and reported the shear behaviour of these systems were we show that the flexynes and reflexynes have very low shear moduli, a property which regrettably limits the prospects of these systems in many practical applications. Finally we examine the in-plane off-axis mechanical properties of the systems and we report that in general, these mechanical properties are highly dependent on the direction of loading. We also find that the auxeticity exhibited by the reflexynes on-axis is lost when these systems are loaded off axis since the Poisson’s ratios becomes positive very rapidly as the structure is stretched slightly off-axis (*e.g.*

15deg off-axis). This is once again of great practical significance as it highlights another major limitation of these systems in their use as auxetics.

**Keywords:** 2D flexyne polyphenylacetylene networks, 2D reflexyne polyphenylacetylene networks, auxetics, molecular simulations

## 1. Introduction

Most materials (*e.g.* rubber, glass, metals, *etc.*), have a positive Poisson's ratio, meaning that they contract transversely when pulled longitudinally and expand transversely when compressed longitudinally. However a small number of naturally occurring and synthetic substances exhibit the unusual property of doing the opposite, that is, they become wider when stretched and thinner when compressed. These unusual materials are now known as auxetics, a word derived from the Greek *auxetos* meaning "which can be increased" [1], but have also occasionally been referred to as "anti-rubber" [2], "dilational" [3] or "self-expanding" [4].

Mathematically, the Poisson's ratio,  $\nu$ , in the  $XY$  plane cross-section of the materials for loading in the  $X$ -direction is defined as the ratio of a lateral contraction to the longitudinal extension during stretching of a material for specified directions,  $\nu = -\varepsilon_y/\varepsilon_x$ , where  $\varepsilon_y$  is the strain in the transverse  $Y$ -direction and  $\varepsilon_x$  is the strain in the longitudinal  $X$ -direction. For most materials this value is positive since a positive  $\varepsilon_x$  (*i.e.* extension in the  $X$ -direction) is accompanied by a negative  $\varepsilon_y$  (*i.e.* a contraction in the  $Y$ -direction). Also, for most everyday materials, the Poisson's ratios are the same irrespective of the particular cross-section of materials studied, and the direction of loading plane (isotropic). Typical values for Poisson's ratios for commonly used materials include 0.5 for rubbers and for soft biological tissues, 0.45 for lead, 0.33 for aluminium, 0.27 for common steels, 0.1 to 0.4 for cellular solids such as typical polymer foams, and nearly zero for cork [5]. Materials can also be anisotropic which implies that the physical properties of the system depend on the direction of the applied stretching. For instance, in some crystals, the Poisson's ratio  $\nu$  can be positive in one direction and negative in another.

The first mention of a material with a negative Poisson's ratio dates back to 1944 when it was reported that crystals of iron pyrite exhibited a negative Poisson's ratio [6]. However, this was treated as an anomaly and the study of materials with negative Poisson's ratio only took off in the 1980's, with auxetic behaviour being experimentally measured or predicted in various types of materials such as foams, [5, 7–11] nano-structured and liquid crystalline polymers [1, 12, 4, 13–15], micro structured polymers [16–18], cubic materials [19] and zeolites [20]. Despite considerable progress in this field which is evidenced by the growth in literature in the last couple of decades, the design and synthesis of materials with  $\nu < 0$  still remain somewhat of a real challenge. Since these materials are quite rare in nature and extremely useful, the impetus for them to be designed, studied and manufactured is great and has attracted experts such as scientists and engineers.

Auxetic materials are not only interesting scientifically for their rare and counter-intuitive elastic behaviour, but also for a number of potentially useful technological applications. For example, for an isotropic material, a negative value of the Poisson’s ratio alters significantly the other mechanical properties. Generally there are four constants which are used to describe the elastic behaviour of an isotropic material and these are the Young’s Modulus ( $E$ ), the shear modulus ( $G$ ), the bulk modulus ( $K$ ) and the Poisson ratio ( $\nu$ ), but these four constants are interdependent through the following relationships:

$$G = \frac{E}{2(1+\nu)} \quad K = \frac{E}{3(1-2\nu)} \quad E = \frac{9KG}{(3K+G)} \quad \nu = \frac{1}{2} \left( \frac{3K-2G}{3K+G} \right) \quad (1)$$

The importance of these four equations lies in the fact, that knowing any two out of the four parameters the third parameter may be obtained by a simple calculation. Furthermore these relationships give a very good picture of the properties of the system.

In spite of all the advantages and new possibilities that these auxetic materials offer together with their uncommon nature, there are still a number of lacunae within the field which are yet to be studied thoroughly. Thus one of the aims of this paper shall be to carry out a theoretical study on 2D polyphenylacetylene “flexyne” and “reflexyne” networked polymers originally reported by Evans *et al.* in 1991 [21] (see Figure 1 for an example) which despite being the subject of various papers, have not been fully characterised as of yet. These polyphenylacetylene networks are of interest since as reported by Evans *et al.* [21] and in various other studies [21–25], the reflexyne networks are predicted to mimic the behaviour of re-entrant hexagonal honeycombs [26, 27] and exhibit negative on-axis Poisson’s ratios.

In this paper the 2D polyphenylacetylene “flexyne” and “reflexyne” networked polymers will be studied using computer based modelling and simulations, a technique which was chosen since so far these networks have not yet been synthesised. In particular, ( $n, m$ )-flexynes and ( $n, m$ )-reflexynes, where,  $m$  and  $n$  are the number of triple bonds on the vertical and side arms of the unit respectively, will be studied.

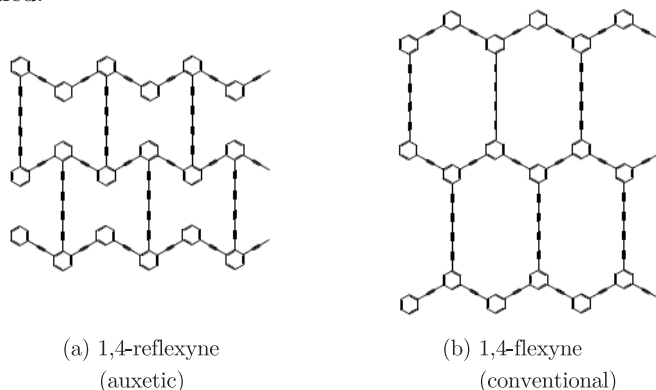


**Figure 1.** (a) Pictorial representation of (1,4)-reflexyne and (b) (1,4)-flexyne

## 2. Simulation methodology

Any modelling experiment involves three distinct stages, namely:

- (a) Defining the system to be modelled;
- (b) Setting up the energy expression and performing an energy minimisation;
- (c) Performing the particular calculations, in this case, simulation of the single crystalline elastic constants.

### 2.1. Defining the system to be modelled

The first stage in any force-field based molecular modelling simulation is to enter the coordinates of the atoms of the system under study into the molecular modelling environment and to define the connectivity of these atoms. This information (*i.e.* the initial coordinates of the atoms and initial definition of the bonds) on which calculations will then be performed shall henceforth be referred to as the starting geometry.

To illustrate the methodology used in this dissertation for constructing the starting geometries of the flexyne and reflexyne networks, we shall discuss in detail the procedure used to construct the (1,4)-flexyne and (1,4)-reflexyne systems.

The conventional and re-entrant infinite periodic honeycomb structures may be constructed using a unit cell which contains two vertical chains and four arm chains as illustrated in Figure 2 (a) and 3 (b), bearing in mind that in the molecular system, each vertex of the honeycomb system represents a phenyl ring whilst the vertical chains and the arm chains represent acetylene chains. The repeat unit of (1,4)-flexyne and (1,4)-reflexyne would be the systems illustrated in Figure 2 (c) and 3 (d), respectively.

These starting geometries in Figure 2 (c) and 3 (d) were entered using the model builder and templates available in *Cerius*<sup>2</sup> through the graphical user interface (GUI). In this procedure, the user inserts all of the atoms into the system and connects them together to define the “bonds” in the systems. This results in a very rough sketch of the system which simply defines the atoms in the model and how these atoms are connected in space (see Figure 3 (a) for the initial structure for (1,4)-flexyne). The “Clean” function was then used to make the model look more realistic (see Figure 3 b). These atoms were then aligned in the  $y$ - $z$  plane (see Figure 3 c), *i.e.* with the vertical ribs aligned parallel to the  $z$ -axes. This alignment was selected because in *Cerius*<sup>2</sup>, crystals are aligned in such a way that:

- The [001] crystal direction is always fixed parallel to the  $Z$  “global” direction;
- The [010] crystal direction always lies in the  $YZ$  plane;
- The [100] crystal direction is free and as a result it may assume any direction.

Thus, by aligning the flexyne basic unit in this way, the user can be sure that the crystal is always aligned to the  $YZ$  plane with the vertical ribs remaining parallel to the  $Z$ -direction.

These systems (which could be thought of as the monomers of infinitely large networked polymers) were then converted into a crystal using the crystal

building module. The initial cell parameters were set as  $\alpha = \beta = \gamma = 90$  deg whilst  $a$  was set to  $4\text{\AA}$ ,  $b = 11\text{\AA}$  and  $c = 35\text{\AA}$  for (1,4)-reflexyne and  $c = 30\text{\AA}$  for (1,4)-flexyne. The choice for the values of  $b$  and  $c$  was made on visual observations making sure that the unit cells fit properly within the cell border (see Figure 3d). On the other hand, the choice of  $a$  was based on the fact that for graphite-like systems, the “infinite” sheets are at a distance of about  $3.6\text{\AA}$  from each other. The final step in the inputting of the model involved joining the “free ends” of the acetylene chains to the phenyl ring in adjacent cells to produce the (1,4)-flexyne or (1,4)-reflexyne networks (Figure 3e).

## 2.2. Setting up the energy expression and energy minimization

Once the starting structure was inputted in *Cerius*<sup>2</sup>, it was necessary to set up of the energy expression. The energy expression is an equation describing the potential energy of the system as a function of its internal / Cartesian coordinates and it is used by the molecular modelling program in the energy minimisation of the system. In this dissertation, various force-fields which have been parameterised for use with hydrocarbons were used, although in this validation study, only the DREIDING 2.21 force-field is considered since all results on the flexyne / reflexyne systems reported in the literature were obtained using this force-field (or earlier versions of it).

The DREIDING 2.21 force-field has an energy expression which is constructed from bonding and non-bond interactions:

$$E^{\text{DREIDING}} = E_{\text{valence}}^{\text{DREIDING}} + E_{\text{non-bond}}^{\text{DREIDING}} \quad (2)$$

where, for the hydrocarbons in our system (which do not have any inversion terms or H-bonding), the valence bond-terms are described by a harmonic bond stretch term, a harmonic angle bending term and a dihedral torsion angle term, whilst the non-bond terms are described by the standard Columbic term and the Lennard-Jones 12-6 VDW potential, *i.e.*:

$$E_{\text{valence}}^{\text{DREIDING}} = \sum_{\substack{\text{all bond} \\ \text{lengths}}} \frac{1}{2} k_s (l - l_0)^2 + \sum_{\substack{\text{all bond} \\ \text{angles}}} \frac{1}{2} k_h (\theta - \theta_0)^2 + \sum_{\substack{\text{all torsion} \\ \text{angles}}} \left\{ \frac{1}{2} B_j [1 - d_j \cos(n_j \phi)] \right\} \quad (3)$$

$$E_{\text{non-bond}}^{\text{DREIDING}} = \frac{q_i q_j}{\epsilon r_{ij}} c + \left[ \frac{A_{ij}}{r_{ij}^{12}} - \frac{B_{ij}}{r_{ij}^6} \right] \quad (4)$$

where all terms have their usual meaning.

It is important to note that this force-field, despite having a term for the Columbic interactions, does not contain any information relating to the partial atomic charges of the system that are needed for use with this term. Instead, these partial charges have to be computed through a separate method. In this dissertation, these charges were computed using the Charge-Equilibration

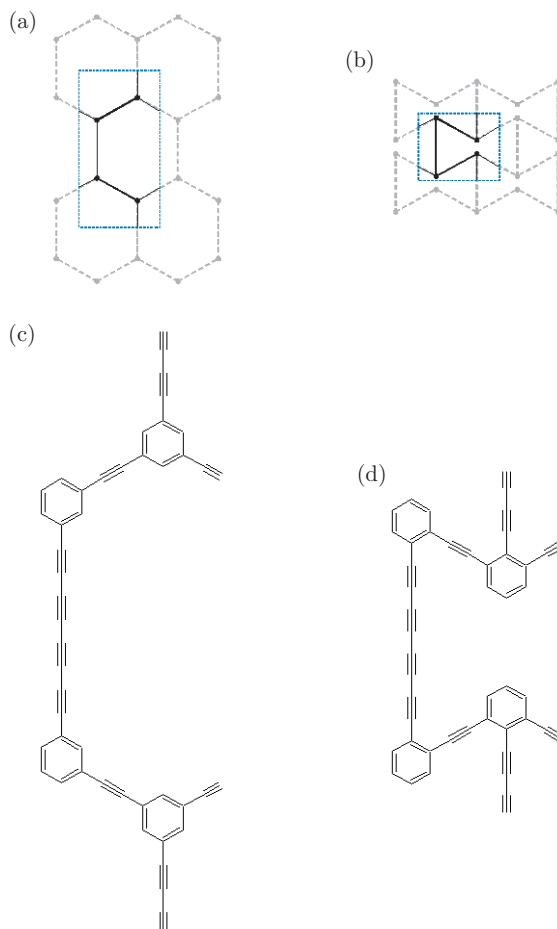


**Figure 2.** A figure showing the arrangement in space of the conventional (a) and re-entrant honeycombs (b), respectively, and the starting geometries as inputted into *Cerius<sup>2</sup>*, (c) and (d) respectively

procedure developed by Rappe *et al.* [28]. This procedure was chosen in preference to the older but still widely in use Gasteiger-Marsili method since the Gasteiger-Marsili method is not recommended for use with delocalized systems, *i.e.* systems which are similar to the ones discussed in this dissertation.

Furthermore, due to the fact that our systems are actually representing an infinite amount of atoms (*i.e.* they are periodic systems), it is not possible to include all of the atom pairs for constructing the non-bond part of the energy expression since there is an infinite amount of these terms. In order to decrease the computational time the amount of non-bond pair terms that are included is truncated by applying cut-offs. *Cerius<sup>2</sup>* has three methods for doing this namely the “Direct method”, the “Spline method” and the “Ewald method”. The Direct method calculates non-bond interaction energies for all atom pairs whose members are closer than some cut-off distance. This method is generally not recommended,

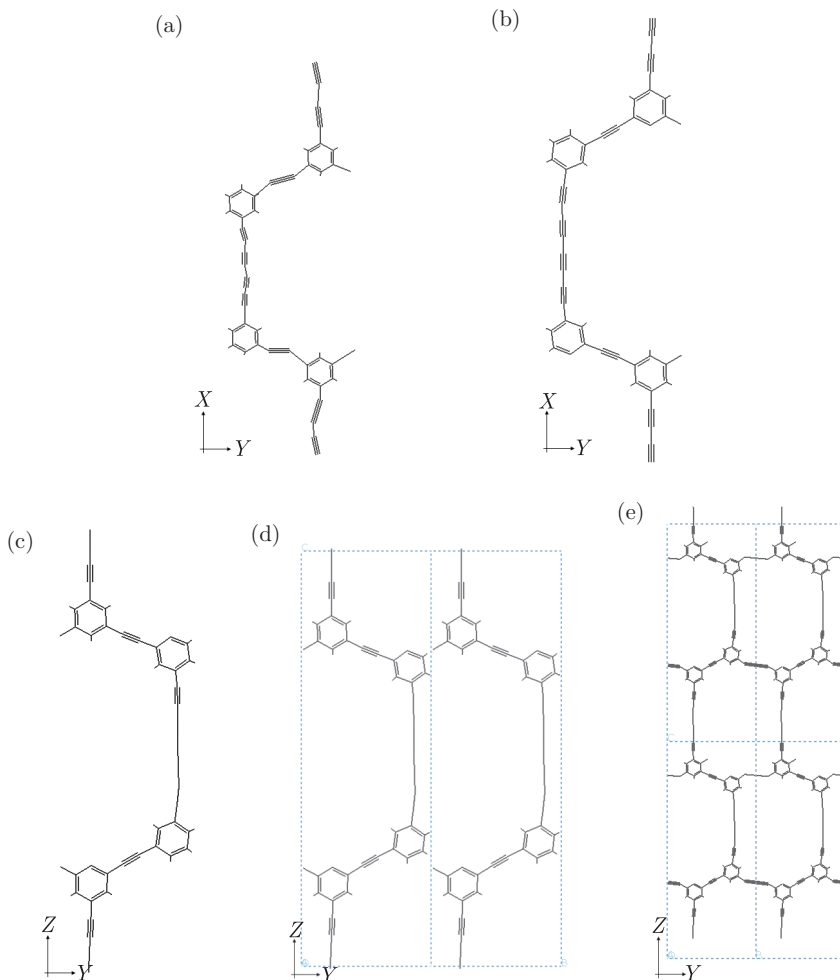


**Figure 3.** A set of figures showing the different stages in the modelling of (1,4)-flexynes, namely the (a) un-cleaned structure (b) cleaned structure (c) structure aligned to the  $YZ$  plane (d) built crystal and (e) the unit cells joined together to form an infinite tessellation

except for small models, for which the cut-off distance should be set to a large enough value that *all* interactions are calculated. Similarly, the Spline method calculates non-bond interaction energies for all atom pairs whose members are closer than the spline-on distance. The interaction energy is gradually attenuated (by a spline function) from its full value to zero as atom-atom distances go from the spline-on to the spline-off distance. The interaction energy is set to zero for atom-atom distances greater than the spline-off distance. A non-bond list, where the atom pairs to be considered in the calculation are listed, is used with the Spline method for faster calculation with most models. However, whilst the “spline cut-offs” work very well for non-periodic models, it has been shown that better results for periodic systems (*i.e.* the systems modelled in this paper)

can be obtained using the “Ewald Summation” technique [29–31]. In the Ewald Summation Method the Coulombic interactions and attractive van der Waals interactions are calculated by the Ewald method [32, 33], while the repulsive van der Waals interactions (which fade out quickly with distance) are calculated by the direct method (described previously). A non-bond list must be used with this method. Since the Ewald summation technique is recommended for periodic models and preferred over the spline method, in this dissertation we shall be using this technique for curtailing the non-bond part of the energy expression. (Note that the Ewald technique cannot be used for non periodic models.)

The energy expression was set up using all parameters, functional forms and settings as set by default in the DREIDING 2.21 force-field with the exception of partial charges which were computed using the Charge Equilibration procedure by Rappe *et al.* and using the Ewald technique for curtailing the non-bond part of the energy expression as described. An energy minimisation of the system was then applied to the system(s). This process involves small adjustments of the conformation (iterations) in order to lower the energy of the system using minimisation algorithms (minimisers). In reality, the number of iterations, or conformation adjustments may range from one to several thousands. Therefore the time needed to carry out a minimisation depends, amongst other things, on the size of the system, the type of minimisation algorithm and the energy expression itself. In *Cerius*<sup>2</sup>, the user can choose from a number of available minimisers based on the steepest descent algorithm, the conjugate gradient algorithm which was used in this dissertation and more accurate Newton-Raphson methods. The program also features the “SMART minimiser” which makes use of several minimisation algorithms which are implemented into the workbench sequentially, starting from the coarse Steepest Descent minimiser and going down to finer minimisers such as the Newton-Raphson. This switching is done automatically as the minimisation proceeds (though the user can pre-select the criteria for switching) and ensures that iterations at a particular level which do not show any progress can be discontinued in favour of more fruitful iterations. This minimiser was used in this paper.

Finally it is important to note that minimisers can only give numerical solutions and the exact location of the minimum is unlikely to be identified. Therefore, a set of pre-defined convergence criteria (also known as termination criteria) have to be used to stop the minimisation once the criteria are satisfied. These convergence criteria indicate how close the calculation is to the exact minimum point, and the higher (*i.e.* stricter) the convergence criteria are, the longer it will take for these criteria to be satisfied with the benefit that the simulated minimum would be closer to the true minimum. The most common method for defining the convergence criteria is to specify the root mean square of the derivative of the energy expression (RMS force) as being less than a particular value. Furthermore, a maximum number of iterations is also set, and minimisation is normally stopped after the earlier of either reaching the convergence criteria or the maximum number of iterations.



**Table 1.** The values of the different termination criteria used by *Cerius<sup>2</sup>*

Convergence criteria	Moderate	Standard	High
RMS force (kcal mol <sup>-1</sup> Å <sup>-1</sup> )	0.50000	0.10000	0.00100
Max force (kcal mol <sup>-1</sup> Å <sup>-1</sup> )	2.50000	0.50000	0.00500
Energy difference (Kcal mol <sup>-1</sup> )	0.00200	0.00100	0.00010
RMS displacement (Å)	0.01000	0.00300	0.00001
Max displacement (Å)	0.05000	0.01500	0.00005
Max stress (GPa, only for periodic systems)	0.50000	0.10000	0.00100
RMS stress (GPa, only for periodic systems)	2.50000	0.50000	0.00500

In *Cerius<sup>2</sup>*, the user may choose to use (in isolation, or in combination) various convergence conditions. It also defines default medium and high convergence criteria (see Table 1).

The minimisations were required to prepare the system for deriving the single crystalline elastic constants. In such simulations, particularly when using the second derivative method, it is essential that the energy minimum is properly identified, and hence high convergence criteria must be used.

It is important to note that to calculate the partial charges of the system correctly through the charge-equilibration procedure, the partial charges must be updated as the energy minimisation proceeds, *i.e.* as the positions of the atoms are updated along the path to the energy minimum. This is due to the fact that the computed charges through Rappe's charge-equilibration procedure depend not only on the connectivity but also the actual position of the atoms.

In view of all this, the following procedure for setting up the energy expression and minimisation was used:

1. Loading of DREIDING 2.21 force-field with default settings with the exception for the method of curtailing the non-bond interactions which was set to the Ewald technique;
2. Calculation of partial charges using the Charge Equilibration procedure;
3. Short energy minimisation using the SMART minimiser up to the earlier of 200 steps or reaching of the *Cerius<sup>2</sup>* default standard convergence criteria;
4. Re-calculation of partial charges using the Charge Equilibration procedure;
5. A second short energy minimisation using the SMART minimiser up to the earlier of 200 steps or reaching of the *Cerius<sup>2</sup>* default standard convergence criteria;
6. Re-calculation of partial charges using the Charge Equilibration procedure;
7. A third energy minimisation using the SMART minimiser up to the earlier of 5000 steps or reaching of the *Cerius<sup>2</sup>* default high convergence criteria;
8. Re-calculation of partial charges using the Charge Equilibration procedure;
9. A fourth and final energy minimisation using the SMART minimiser up to the earlier of 5000 steps or reaching of the *Cerius<sup>2</sup>* default high convergence criteria;

10. Saving the model in order to use it in the determination of the mechanical properties of the system under study (this is explained later on).

These steps were executed through the following script so as to:

- a) Minimise human errors where the possibility of the user skipping a step in a highly repetitive procedure is eliminated;
- b) Reduce the computational time taken by *Cerius*<sup>2</sup>, by running the calculations in background mode.

### 2.3. Calculating the Mechanical (Elastic) Properties

*Cerius*<sup>2</sup> provides three automated methods for calculating the mechanical properties. These are the second derivative method, the constant stress minimisation method and the constant strain minimisation method. Using any of the three methods, the full  $6 \times 6$  set of elastic constants can be computed from which one may obtain all the other mechanical properties (the Young's moduli, shear moduli and Poisson's ratios).

The second derivative method calculates the second derivative of the lattice energy, with respect to the atomic coordinates by performing a single point energy calculation. It computes a symmetric stiffness matrix, since the elements  $c_{ij}$  relate to the second derivative of the energy expression (with respect to strain,  $\varepsilon_i$ ) as follows:

$$C_{ij} = \frac{1}{V} \frac{\partial^2 E}{\partial \varepsilon_i \partial \varepsilon_j} \quad (5)$$

where  $V$  is the volume of the unit cell and  $E$  is the energy of the system.

The constant stress minimisation method calculates the elastic properties from the strain response to a series of applied external stresses and an empirical stress-strain relationship is calculated. *Cerius*<sup>2</sup> employs an automated method where the structure is minimised repeatedly (a sweep) with a series of pre-defined stresses. On the other hand, the constant strain minimisation method carries out sweeps of minimisations at pre-defined strains as opposed to stresses.

In addition to this, the user may also perform a "manual" constant stress minimisation where a number of energy minimisations at different values of applied stress are performed and then the minimised structures at the various stress are used to study the effect of stress on the system. The user, may for example, measure the strains from the unit cell vectors and use these to plot stress-strain plots.

## 3. Simulation of the structure and on-axis mechanical properties of (1,4)-flexyne and (1,4)-reflexyne using the DREIDING force-field

In this section we will use the three automated methods and the "manual constant stress" method will be used to simulate the properties of the (1,4)-flexyne and (1,4)-reflexyne networks.

### 3.1. Simulations

Simulations were carried out using the commercially available *Cerius<sup>2</sup>* Molecular Modelling software (Accelrys, Version 4.10) running on a Silicon Graphics Octane2 workstation running the IRIX 6.4 operating system.

The procedure for calculating the elastic constants through the second derivative method, automated constant strain and automated constant stress methods were driven through the script file (see Script 1). In this script:

- Lines 5–7 load the force-field and define the non-default force-field settings, *i.e.* that the non-bond terms are summed and truncated using the Ewald summation technique;
- Line 9 starts a for/next loop so that lines 10–44 are executed for each of the structures being considered (in this case, twice: first for (1,4)-flexyne and then for (1,4)-reflexyne);
- Line 10 loads the initial unminimised structures; line 12 calculates the partial charges using the Charge Equilibration procedure;
- Lines 14–24 minimise the systems to high convergence criteria using the SMART minimiser. The minimisation is carried out in such a way that the charges are updated as the system is optimised (lines 17, 19);
- Line 25 saves the minimised structures;
- Lines 26–43 simulate the mechanical properties of the minimised systems using the second derivative, automated constant stress and automated constant strain methods.

Script 1 was then re-run using the conjugate gradient minimisation algorithm by replacing Line 14 with: MECHANICS/METHOD "CONJUGATE GRADIENT".

Note that in this procedure, for each of the two minimisers used, the mechanical properties are calculated three times (*i.e.* six times in total for each structure). Furthermore, it is important to note that despite the fact that the program allows the user to control various settings, in most cases, the default settings were suitable for the simulations. In fact, with the Second derivative method (lines 26–30), the default settings were used throughout whilst in the automated Constant Stress/Strain methods (lines 31–36 and 37–43), the only setting which was altered was the parameter that 11 points would be used for the calculation of each of the six stress-strain curves<sup>1</sup>: five in compression, five in tension and one at zero stress. The default settings were used for the rest of the options.

---

1. With these settings, the procedure involves 66 minimisations for each constant stress or constant strain simulation. The default setting is to use only two points for each stress-strain curve which, despite being sufficient for plotting a straight line graph, would fail to give an indication of any errors.

```

1  #Setting directories#
2  set home ''/usr/chem/lara05''
3  set msi ''/software/accelrys/cecius2_c410/Cerius2-Resources''
4  #Loading ff and assigning of non-default ff settings#
5  FORCE-FIELD/LOAD_FORCE_FIELD ''${msi}/FORCE-FIELD/DREIDING2.21''
6  FORCE-FIELD/LONG_RANGE_METHOD_VDW EWALD
7  FORCE-FIELD/LONG_RANGE_METHOD_COULOMB EWALD
8  #'Foreach' loop to run script twice, once for each structure#
9  foreach STR {14F 14R} {
10 FILES/LOAD
    ''${home}/Chapter3_initial_structures/${STR}_INIT.msi''
11 #Charge equilibration#
12 CHARGE/CALCULATE
13 #Minimisation using 200 iterations and calculating the charges#
    #at the end of each minimisation#
14 MECHANICS/METHOD ''SMART MINIMISER''
15 MECHANICS/MAX_ITERATIONS 200
16 MECHANICS/MINIMIZE
17 CHARGE/CALCULATE
18 MECHANICS/MINIMIZE
19 CHARGE/CALCULATE
20 #High convergence minimisation using 5000 iterations#
21 MECHANICS/MAX_ITERATIONS 5000
22 MECHANICS/CONV_LEVEL ''HIGH CONVERGENCE''
23 MECHANICS/MINIMIZE
24 MECHANICS/MINIMIZE
25 FILES/SAVE ''${home}/Chapter3_results/${STR}_min.msi''
26 #Second Derivative Calculation#
27 MECHPROPS/MINIMIZE_FIRST NO
28 MECHPROPS/ACCUMULATE_AVERAGES NO
29 #Saving the output from the Second Derivative Calculation#
30 MECHPROPS/NAMES_ROOT ''${home}/CH3/MP_SD_${STR}''
31 #Constant Stress Calculation#
32 MECHPROPS/CALCULATE
33 MECHPROPS/METHOD ''CONST STRESS MIN''
34 MECHPROPS/STRESS_MIN_NO_POINTS 11
35 #Saving the output from the Constant Stress Calculation#
36 MECHPROPS/NAMES_ROOT ''${home}/CH3_/MP_CSTRESS_${STR}''
37 #Constant Strain Calculation#
38 MECHPROPS/CALCULATE
39 MECHPROPS/METHOD ''CONST STRAIN MIN''
40 MECHPROPS/STRAIN_MIN_NO_POINTS 11
41 #Saving the output from the Constant Strain Calculation#
42 MECHPROPS/NAMES_ROOT
    ''${home}/Chapter3_initial_structures/MP_CSTRAIN_${STR}''
43 MECHPROPS/CALCULATE
44 }

```

**Script 1.** The script which minimises the initial structures and then simulates their mechanical properties using the Second Derivative, automated Constant Stress and automated Constant Strain methods

Finally, we also simulated the mechanical properties in the  $YZ$  plane<sup>2</sup> using the “manual constant strain method” where:

- (a) tensile/compressive stresses in the range of  $\pm 5\%$  were applied in the  $Y$ - and the  $Z$ -direction in order to be able to obtain the Young’s moduli ( $E_y$  and  $E_z$ ), the Poisson’s ratios ( $\nu_{yz}$  and  $\nu_{zy}$ ) and shear coupling coefficients ( $\eta_{xz}$  and  $\eta_{yz}$ );
- (b) shear stresses in the  $ZY$  plane were applied in the range of  $\pm 0.05$  GPa at 0.01 GPa intervals in order to be able to obtain the shear modulus ( $G_{zy}$ ) and the shear coupling coefficients ( $\eta_{zx}$  and  $\eta_{zy}$ ).

This procedure was also carried out by Script 2. In this script:

- Lines 1–10 load the DREIDING 2.21 force-field as explained in section 3.2.1 (b);
- Lines 11–14 create the folders needed to save the files produced from this simulation;
- Line 16 loads the system under study (taken from Script 1);
- Lines 18–29 define the stresses and their direction<sup>3</sup>;
- Lines 30–43 minimise the system under the applied stresses as explained in section 3.2.1b;
- Line 44 saves the minimised systems under the applied stress in the .msi format.

The files created in line 44 contain the unit shape matrix, from which the unit cell projections in the  $X$ ,  $Y$  and  $Z$  directions can be calculated. In *Cerius2*, the unit cell relates to the Cartesian axis by having the cell vector  $c$  parallel to the  $Z$ -axis, and  $b$  in the  $YZ$  plane. With these constraints, the cell matrix  $\mathbf{H}$  is an upper triangular matrix:

$$\mathbf{H} = \begin{bmatrix} h_{11} & h_{12} & h_{13} \\ 0 & h_{22} & h_{23} \\ 0 & 0 & h_{33} \end{bmatrix} \quad (6)$$

where  $h_{ij}$  relate to the unit cell vectors  $\mathbf{a}$ ,  $\mathbf{b}$  and  $\mathbf{c}$  through

$$\begin{aligned} \mathbf{a} &= h_{11}\mathbf{i} + h_{12}\mathbf{j} + h_{13}\mathbf{k} \\ \mathbf{b} &= h_{22}\mathbf{j} + h_{23}\mathbf{k} \\ \mathbf{c} &= h_{33}\mathbf{k} \end{aligned} \quad (7)$$

Thus, the projections of the unit cell in the  $X$ ,  $Y$  and  $Z$ -directions respectively are  $h_{11}$ ,  $h_{22}$ , and  $h_{33}$ .

The unit shape matrix for the system under different loads was then extracted to a single file. This procedure was also carried out using Script 3. In this script

2. Since the analysis of the data obtained from this method is fairly time consuming, we will only simulate the properties in the plane of the structure, *i.e.* the  $YZ$  plane, which is the main plane of interest.

3. Note that the systems were found to exhibit different properties in tension and compression (see discussion). Thus, Line 18 was modified to suit the system being modelled.

```

1  #Setting directories#
2  set home ``/usr/chem/lara05``
3  set msi ``/software/accelrys/cerius2_c410/Cerius2-Resources``
4  #Running the script for the various load directions and ff#
5  Foreach FORC {LOAD_Y} {
6  FORCE-FIELD/LOAD_FORCE_FIELD ``${msi}/FORCE-FIELD/$DREIDING2.21``
7  FORCE-FIELD/LONG_RANGE_METHOD_VDW EWALD
8  FORCE-FIELD/LONG_RANGE_METHOD_COULOMB EWALD
9  #Running the script for the various structures under study#
10 Foreach STR {14F} {
11 #Setting up the Folders#
12 !mkdir ${home}/manual_stress_fin/ DREIDING2.21
13 !mkdir ${home}/manual_stress_fin/ DREIDING2.21/${STR}
14 !mkdir ${home}/manual_stress_fin/ DREIDING2.21/${STR}/${FORC}
15 #Loading the initial structure#
16 FILES/LOAD
   ``${home}/Chapter3_initial_structures/${STR}_INIT.msi``
17 #Running the script for various loads#
18 Foreach LOAD {{0.00 0.56 1.12 1.68 2.24 2.80}} {
19 #Applying the load in the appropriate direction#
20 If {$FORC == ``LOAD_Y``} {
21 MECHANICS/3D_STRESS ``0`` ``${LOAD}`` ``0`` ``0`` ``0`` ``0``
22 set direct ``y``
23 } elseif {$FORC == ``LOAD_Z``} {
24 MECHANICS/3D_STRESS ``0`` ``0`` ``${LOAD}`` ``0`` ``0`` ``0``
25 set direct ``z``
26 } else {$FORC == ``SHEAR_ZY``} {
27 MECHANICS/3D_STRESS ``0`` ``0`` ``0`` ``${LOAD}`` ``0`` ``0``
28 set direct ``zy``
29 }
30 #Charge equilibration#
31 CHARGE/CALCULATE
32 #Minimisation using 200 iterations and calculating the charges#
   #at the end of each minimisation#
33 MECHANICS/METHOD ``SMART``
34 MECHANICS/MAX_ITERATIONS 200
35 MECHANICS/MINIMIZE
36 CHARGE/CALCULATE
37 MECHANICS/MINIMIZE
38 CHARGE/CALCULATE
39 #High convergence minimisation using 5000 iterations#
40 MECHANICS/MAX_ITERATIONS 5000
41 MECHANICS/CONV_LEVEL ``HIGH CONVERGENCE``
42 MECHANICS/MINIMIZE
43 MECHANICS/MINIMIZE
44 FILES/SAVE ``${home}/manual_stress_fin/DREIDING2.21/${STR}/
   ${FORC}/${STR}_${LOAD}_${direct}.msi``
45 } } }

```

**Script 2.** The script used to simulate the mechanical properties using the ‘manual constant strain’ method, where LINE 18 defines the loads in the particular direction being studied. This line is defined according to structure being modelled, the direction of measurement and whether the loads are in tension or compression

- Line 1: the script is defined as command shell file;
- Lines 4–9: the loads used in the previous simulation are entered in the variables  $s1, s2, \dots, s6$ ;
- Lines 10–13: the script is instructed to loop for the various load directions and structures used in this study;
- Lines 14–24: the variable “direct” is given its appropriate value;
- Line 25: the folder path where the files were saved in the previous simulations is defined;
- Line 26: a new file named “Res\_short.res” is created;
- Lines 27–28: the script is instructed to loop for the various loads applied on the system under study;
- Lines 29–33: the unit cell projection recorded in the previous simulations are extracted and saved in the “Res\_short.res” created previously.

This data extracted from the unit cell shape matrix of the system under study at different loads was then plotted as strain-strain and stress-strain plots and from these plots the Poisson’s ratios, coupling coefficients, Young’s Moduli and shear modulus in the  $YZ$  plane were calculated.

In particular,

- (a) The Poisson’s ratios were obtained from a strain – strain relation since:

$$\nu_{ij} = -\frac{\varepsilon_j}{\varepsilon_i} \quad (\text{where } i, j = y, z)$$

- (b) The coupling coefficients were obtained from a shear strain – tensile strain relation since:

$$\eta_{iz} = \frac{\gamma_{zy}}{\varepsilon_i} \quad \text{and} \quad \eta_{zi} = \frac{\varepsilon_i}{\gamma_{zy}} \quad (\text{where } i, j = y, z)$$

- (c) The Young’s modulus were obtained from a tensile stress – strain relation since:

$$E_i = \frac{\sigma_i}{\varepsilon_i} \quad (\text{where } i = y, z)$$

- (d) the shear modulus was obtained from a shear stress – strain relation since:

$$G_{zy} = \frac{\tau_{zy}}{\gamma_{zy}} \quad (\text{where } i = y, z)$$

Note that together, these properties make up the “full  $3 \times 3$  compliance sub-matrix”  $\mathbf{S}$ :

$$\mathbf{S} = \begin{pmatrix} s_{11} & s_{12} & s_{13} \\ s_{21} & s_{22} & s_{23} \\ s_{31} & s_{32} & s_{33} \end{pmatrix} = \begin{pmatrix} \frac{1}{E_y} & \frac{-\nu_{21}}{E_z} & \frac{\eta_{31}}{G_{zy}} \\ \frac{-\nu_{12}}{E_y} & \frac{1}{E_z} & \frac{\eta_{32}}{G_{zy}} \\ \frac{\eta_{13}}{E_y} & \frac{\eta_{23}}{E_z} & \frac{1}{G_{zy}} \end{pmatrix} = \begin{pmatrix} \frac{\varepsilon_y}{\sigma_y} & \frac{\varepsilon_y}{\sigma_z} & \frac{\varepsilon_y}{\tau_{zy}} \\ \frac{\varepsilon_z}{\sigma_y} & \frac{\varepsilon_z}{\sigma_z} & \frac{\varepsilon_z}{\tau_{zy}} \\ \frac{\gamma_{zy}}{\sigma_y} & \frac{\gamma_{zy}}{\sigma_z} & \frac{\gamma_{zy}}{\tau_{zy}} \end{pmatrix}$$

which can then be transformed to obtain the off-axis properties.

```

1  #!/bin/sh
4  s1=0.05
5  s2=0.04
6  s3=0.03
7  s4=0.02
8  s5=0.01
9  s6=0

10 for FORC in ''LOAD_Y'' ''LOAD_Z'' ''SHEAR_ZY''
11 Do
12   for STR in ''14F'' ''14R''
13   do
14     if [ $FORC ''LOAD_Y'' ] ; then
15       direct = ''y''
16     else
17       if [ $FORC ''LOAD_Z'' ] ; then
18         direct = ''z''
19       else
20         if [ $FORC ''SHEAR_ZY'' ] ; then
21           direct = ''zy''
22         fi
23       fi
24     fi

25     Pth=/usr/chem/lara05/manual_stress_fin/DREIDING2.21/${STR}/
26     ${FORC}/
27     echo ''Projections'' >${pth}RES_short.res
28     for stre in -$s1 -$s2 -$s3 -$s4 -$s5 $s6 $s5 $s4 $s3 $s2 $s1
29     do
30       echo '''' >>${pth}RES_short.res
31       echo ''${STR}_${stre}_${direct}'' >>${pth}RES_short.res
32       echo '''' >>${pth}RES_short.res

33       sed -n -e ''4,6w ${pth}${STR}_${stre}_${direct}.res''
34       ${pth}${STR}_${stre}_${direct}.msi
35       cat ${pth}${STR}_${stre}_${direct}.res >>${pth}RES_short.res
36     done
37   done
38 Done

```

**Script 3.** The script file used to extract the unit shape matrix from the .msi files

### 3.2. Results and Discussion

It was noted that all minimisations carried out prior to calculation of the elastic constants were performed to completion and in less than 1 minute (see Table 2). Also, it was found that the time taken for the different automated<sup>4</sup> simulations depended significantly on the method used for simulating the simulation as detailed in Table 2.

---

4. Since the “manual constant strain” method is mostly time consuming in the data analysis stage which has to be done manually by the user, comparison times are presented only for the automated methods where the results are generated by the programme.



**Table 2.** The time taken for the simulations when using (a) the conjugate-gradient minimiser, and (b) the SMART minimiser

	Time taken (minutes, seconds)	
	(1,4)-flexyne	(1,4)-reflexyne
Minimisation (lines 13–24)	(a) 9s (b) 15s	(a) 45s (b) 5s
Computation of the mechanical properties through second derivative method (lines 27–30)	(a) 1s (b) 1s	(a) 1s (b) 1s
Computation of the mechanical properties through automated constant stress method (lines 32–36)	(a) 49m 52s (b) > 2 days*	(a) 40m 56s (b) > 2 days*
Computation of the mechanical properties through automated constant strain method (lines 38–43)	(a) 3m 4s (b) 9h 43m	(a) 3m 7s (b) N/A

\* Note that when using the conjugate gradient minimiser all simulations were executed to completion. However when using the smart minimiser, the automated constant stress method took a very long time, and was discontinued after 48 hours from its initiation

Table 2 shows very clearly that when comparing the three automated methods, the Second Derivative method was the fastest followed by the automated constant strain method which was much slower. This substantial increase in the computational time is due to the fact that for the constant stress method and similarly for the constant strain method, the process involved sixty-six minimisations, *i.e.* eleven for each of the six independent elements of the stress vector (three axis stresses and three shear stresses).

In the case of the automated constant stress method, when using the conjugate gradient minimiser, the simulations were *c.* 16 times slower than the automated constant strain method and *c.* 3000 times slower than the second derivative method. When using the SMART minimiser, the automated constant strain method took an even longer time to complete (about 350 times more than when using the conjugate gradient method). Moreover, as stated in Table 2, the automated constant stress simulations took so long, that after 48 hours they had to be discontinued by the user. The reason for the increase in duration when using the SMART minimiser is probably that the SMART minimiser makes use of variants of the Newton-Raphson method which are very computationally intensive [34].

Table 3 and Table 4 show a comparison of the on-axis mechanical properties, *i.e.* the three Young's moduli, the six Poisson's ratios and the three shear moduli with each other and to published data (where available). These results show very clearly that despite the very big differences in the computational times, the three automated methods give very comparable results, and that irrespective of the computational method used, (1,4)-flexyne exhibits positive on-axis Poisson's ratios whilst (1,4)-reflexyne exhibits negative on-axis Poisson's ratios in the  $YZ$  plane, *i.e.* the plane of the honeycombs. For example, in the case of (1,4)-flexyne, all three methods gave results within the range of  $0.85 \pm 0.03$  for  $\nu_{zy}$  and  $0.34 \pm 0.02$  for  $\nu_{yz}$  whilst in the case of (1,4)-reflexyne, the range for  $\nu_{zy}$  was from  $-0.28 \pm 0.02$  whilst for  $\nu_{yz}$ , the range was  $-0.37$  to  $-0.38$ . Furthermore, these values were also

**Table 3.** (a) The mechanical properties of (1,4)-flexynes as computed by the various methods described above *i.e.* the Second Derivative, (SD) automated Constant Stress (ACS), automated Constant Strain (ACE) method and manual constant stress (MCS) methods and compared with previously reported results. N//A indicates that no data is available while N/C indicates that the data was not computed. NOTE that \* indicates that the values were not computed since the system failed at very low loads

	Young's moduli (GPa)				Poisson's ratios								Shear Moduli (GPa)		
	$E_x$	$E_y$	$E_z$	$\nu_{xy}$	$\nu_{yx}$	$\nu_{zx}$	$\nu_{xz}$	$\nu_{yz}$	$\nu_{zy}$	$G_{xy}$	$G_{yz}$	$G_{xz}$			
Published data	Evans(1995)	N//A	56.2	160	N//A	N//A	N//A	0.32	0.9	N//A	N//A	N//A			
	Alderson(2005b)	N//A	54.6	140	N//A	N//A	N//A	0.34	0.88	N//A	N//A	N//A			
Conjugate Gradient minimiser	SD	6.45	55.63	142.83	-0.01	-0.05	0.05	0.34	0.88	0.22	3.29	-0.02			
	ACS	7.61	58.94	143.95	-0.33	0.22	-0.42	0.35	0.82	0.00	3.32	0.00			
	ACE	6.87	57.97	148.72	0.00	0.09	-0.06	0.00	0.86	0.24	5.30	-0.01			
	MCS (Tension)	N//A	62.53	158.91	N//A	N//A	N//A	N//A	0.34	0.91	N//A	2.85			
	MCS (Compres.)	N//A	53.42	*	N//A	N//A	N//A	N//A	0.35	*	N//A	2.92			
	MCS (Average)	N//A	59.44	*	N//A	N//A	N//A	N//A	0.34	*	N//A	3.36			
SMART minimiser	SD	5.62	55.78	143.12	0.00	-0.02	-0.05	0.00	0.34	0.88	0.21	0.03			
	ACS	N//A	N//A	N//A	N//A	N//A	N//A	N//A	N//A	N//A	N//A	N//A			
	ACE	6.44	55.63	142.98	0.00	-0.04	0.04	0.00	0.34	0.88	0.21	0.01			
	MCS (Tension)	N//A	62.27	159.17	N//A	N//A	N//A	N//A	0.34	0.91	N//A	3.30			
	MCS (Compres.)	N//A	56.99	133.07	N//A	N//A	N//A	N//A	0.33	0.91	N//A	3.31			
	MCS (Average)	N//A	61.29	156.65	N//A	N//A	N//A	N//A	0.34	0.91	N//A	3.30			

**Table 3 – continued.** (b) The  $R^2$  values obtained for the manual constant stress method.

		Young's moduli (GPa)			Poisson's ratios						Shear Moduli (GPa)		
		$E_x$	$E_y$	$E_z$	$\nu_{xy}$	$\nu_{yx}$	$\nu_{zx}$	$\nu_{xz}$	$\nu_{yz}$	$\nu_{zy}$	$G_{xy}$	$G_{yz}$	$G_{xz}$
Conjugate Gradient minimiser	MCS (Tension)	N//A	0.9991	0.9989	N//A	N//A	N//A	N//A	0.9999	0.9999	N//A	0.9450	N//A
	MCS (Compres.)	N//A	0.9979	*	N//A	N//A	N//A	N//A	0.9938	*	N//A	0.9475	N//A
	MCS (Average)	N//A	0.9985	*	N//A	N//A	N//A	N//A	0.9997	*	N//A	0.9668	N//A
SMART minimiser	MCS (Tension)	N//A	0.9989	0.9990	N//A	N//A	N//A	N//A	1.0000	1.0000	N//A	1.0000	N//A
	MCS (Compres.)	N//A	0.9994	0.9972	N//A	N//A	N//A	N//A	0.9984	0.9996	N//A	1.0000	N//A
	MCS (Average)	N//A	0.9992	0.9992	N//A	N//A	N//A	N//A	1.0000	1.0000	N//A	1.0000	N//A

**Table 4.** (a) The mechanical properties of (1,4)-reflexynes as computed by the various methods described above *i.e.* the Second Derivative, (SD) automated Constant Stress (ACS), automated Constant Strain (ACE) method and manual constant stress (MCS) methods and compared with previously reported results. N//A indicates that no data is available while N/C indicate that the data was not computed.

	Young's moduli (GPa)			Poisson's ratios						Shear Moduli (GPa)		
	$E_x$	$E_y$	$E_z$	$\nu_{xy}$	$\nu_{yx}$	$\nu_{zx}$	$\nu_{xz}$	$\nu_{yz}$	$\nu_{zy}$	$G_{xy}$	$G_{yz}$	$G_{xz}$
Published data	Evans(1995)	N//A	124	N//A	N//A	N//A	N//A	N//A	-0.29	N//A	N//A	N//A
	Alderson(2005b)	N//A	N//A	N//A	N//A	N//A	N//A	N//A	N//A	N//A	N//A	N//A
Conjugate Gradient minimiser	SD	10.64	129.61	102.05	0.02	0.29	-0.04	0.00	-0.37	-0.29	0.69	1.96
	ACS	10.72	133.26	103.60	0.06	0.33	-0.21	0.02	-0.38	-0.26	0.00	2.01
	ACE	10.31	129.04	102.58	0.03	0.33	0.03	-0.01	-0.37	-0.30	0.72	1.88
	MCS (Tension)	N//A	137.72	91.64	N//A	N//A	N//A	N//A	-0.39	-0.29	N//A	1.92
	MCS (Compres.)	N//A	133.68	104.57	N//A	N//A	N//A	N//A	-0.34	-0.28	N//A	1.92
SMART minimiser	MCS (Average)	N//A	136.60	93.12	N//A	N//A	N//A	N//A	-0.39	-0.29	N//A	2.07
	SD	10.01	129.69	101.40	0.02	0.28	-0.08	-0.01	-0.38	-0.29	0.65	1.92
	ACS	N//A	N//A	N//A	N//A	N//A	N//A	N//A	N//A	N//A	N//A	N//A
	ACE	10.10	129.71	101.40	0.02	0.28	-0.07	-0.01	-0.38	-0.30	0.66	1.92
	MCS (Tension)	N//A	136.16	91.18	N//A	N//A	N//A	N//A	-0.39	-0.29	N//A	1.88
MCS (Compres.)	MCS (Compres.)	N//A	129.34	102.16	N//A	N//A	N//A	N//A	-0.37	-0.29	N//A	1.96
	MCS (Average)	N//A	135.24	92.56	N//A	N//A	N//A	N//A	-0.38	-0.29	N//A	1.92

**Table 4 – continued.** (b) The  $R^2$  values obtained for the manual constant stress method

	Young's moduli (GPa)			Poisson's ratios						Shear Moduli (GPa)		
	$E_x$	$E_y$	$E_z$	$\nu_{xy}$	$\nu_{yx}$	$\nu_{zx}$	$\nu_{xz}$	$\nu_{yz}$	$\nu_{zy}$	$G_{xy}$	$G_{yz}$	$G_{xz}$
Conjugate Gradient minimiser	MCS (Tension)	N//A	0.9998	0.9995	N//A	N//A	N//A	N//A	1.0000	0.9994	N//A	0.9235
	MCS (Compres.)	N//A	1.0000	1.0000	N//A	N//A	N//A	N//A	0.9856	0.9990	N//A	0.9974
	MCS (Average)	N//A	0.9998	0.9993	N//A	N//A	N//A	N//A	1.0000	0.9996	N//A	0.9841
SMART minimiser	MCS (Tension)	N//A	0.9998	0.9991	N//A	N//A	N//A	N//A	1.0000	0.9993	N//A	1.0000
	MCS (Compres.)	N//A	1.0000	1.0000	N//A	N//A	N//A	N//A	1.0000	1.0000	N//A	1.0000
	MCS (Average)	N//A	0.9999	0.9993	N//A	N//A	N//A	N//A	1.0000	0.9996	N//A	0.9999

comparable to the ones obtained by Evans *et al.* [22] and Alderson *et al.* [23] thus adding confidence in our modelling methodology.

However, when considering the properties in the other two planes, *i.e.* the  $XY$  and  $XZ$  planes, some of the properties were found to be dependent on the method used. In an attempt to understand more clearly the reason behind these deviations, we analysed the data which is stored by *Cerius*<sup>2</sup> when computing the mechanical properties. In particular, we analysed the data used in generating the stress-strain curves, the gradients of which are used in the computation of the elements of the stiffness/compliance matrices. This data showed that in the cases when the deviations were considerable, the data was very scattered. This was very evident, for example, in the data used for calculating the ‘12’ and ‘13’ elements of the elements which are required for the Poisson’s ratios  $\nu_{xy}$  and  $\nu_{xz}$ , two properties which show considerable deviations, (see Figure 7(a) and (b)) when compared to the data used for calculating the ‘11’ element which is used for calculating  $E_x$  which shows little deviations (see Figure 7c).

An explanation for this “scatter” in the data relating to the  $XY$  and  $XZ$  planes (when compared to the  $YZ$  plane) can be derived by noting the structure of the models. The flexynes/reflexynes are essentially 2D covalent networks aligned in the  $YZ$  plane) which are “loosely” connected together through much weaker non-bond interactions ( $\pi$ - $\pi$ , similar to the interactions holding parallel graphite layers together). This type of bonding results in systems which are “well defined” in the  $YZ$  plane (hence the “lack of scatter” in the data relating to this plane), but which can adopt various “equally good” conformations in the other planes (hence the “scatter”). Evidence for this type of bonding can be found from the facts that:

This weaker bonding which holds together the different layers is also reflected by the fact that the Young’s modulus in the  $X$  direction is significantly lower than that in the other two directions ( $E_x$  is an order of magnitude lower than the other two on-axis moduli) and that the shear moduli  $G_{xy}$  and  $G_{xz}$  are close to zero, indicating that the different layers can easily “slip” past each other.

It is also important to note that even in the  $YZ$  plane, the moduli are such that the shear on-axis modulus is around 30 times lower than the on-axis Young’s moduli. This is a very important consideration since it shows that in reality, these materials are expected to be very weak in shear, a property which will reduce the material’s suitability for many practical applications:

- the separation between the layers is *c.* 3.6Å, typical of graphite like-systems;
- phenyl rings from adjacent layers are stacked “off-centre” from each other as illustrated in Figure 8, a stacking arrangement which is typical of systems exhibiting  $\pi$ - $\pi$  interactions.

These differences in the moduli (*e.g.* the anisotropy between the three Young’s moduli) highlight one of the main weaknesses of the automated constant stress method over the other methods. It is regrettable, that as illustrated in Figure 9, the user of *Cerius*<sup>2</sup> can only define the number of points per sweep and

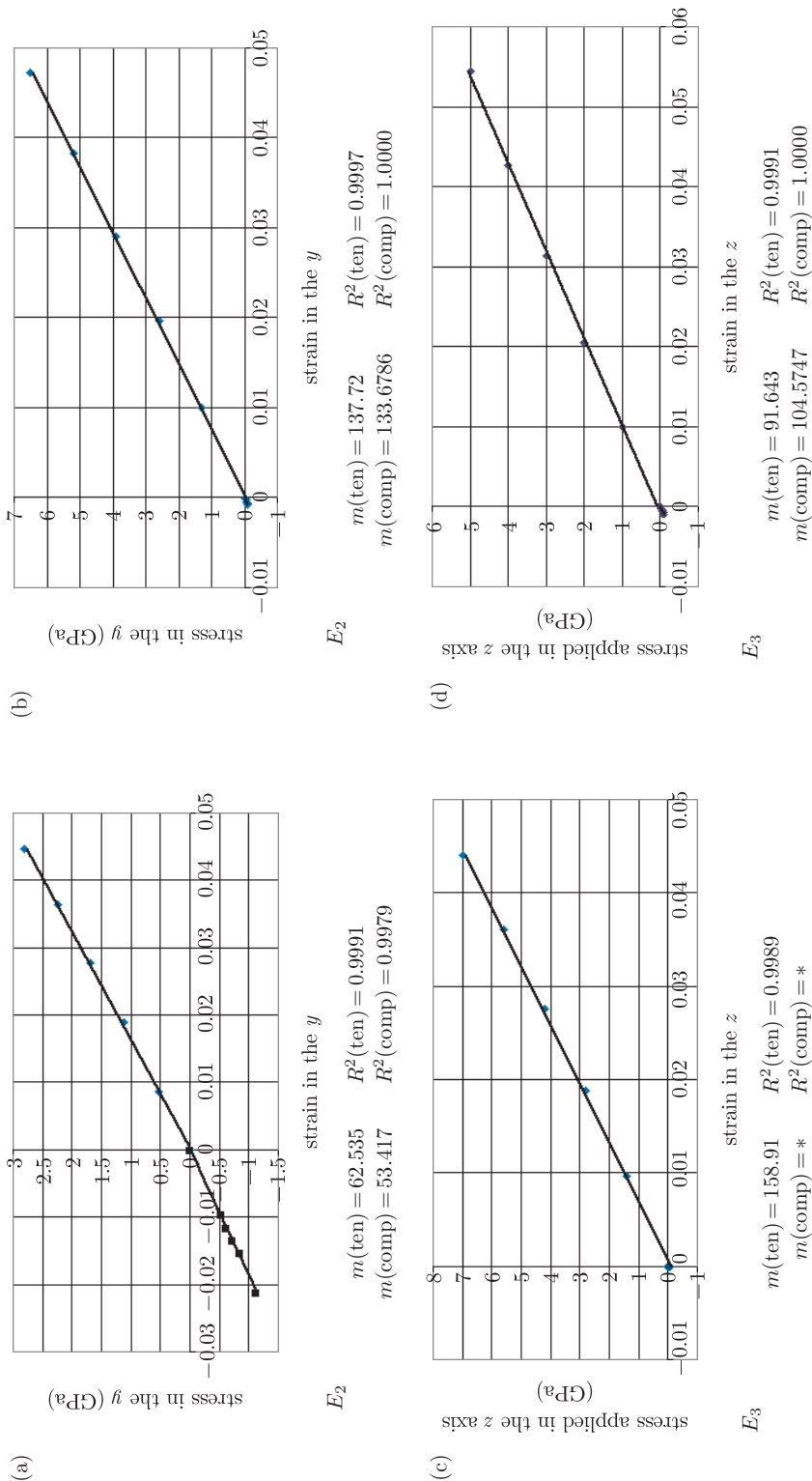


**Figure 4.** The plots obtained for the Young's moduli from the stress-strain plots in the Y & Z direction for (1,4)-flexyne (a) & (c) respectively, and for (1,4)-reflexyne (b) & (d) respectively, using the conjugate gradient method, where  $m$  is the gradient of the plot. NOTE that \* indicates that the values were not computed

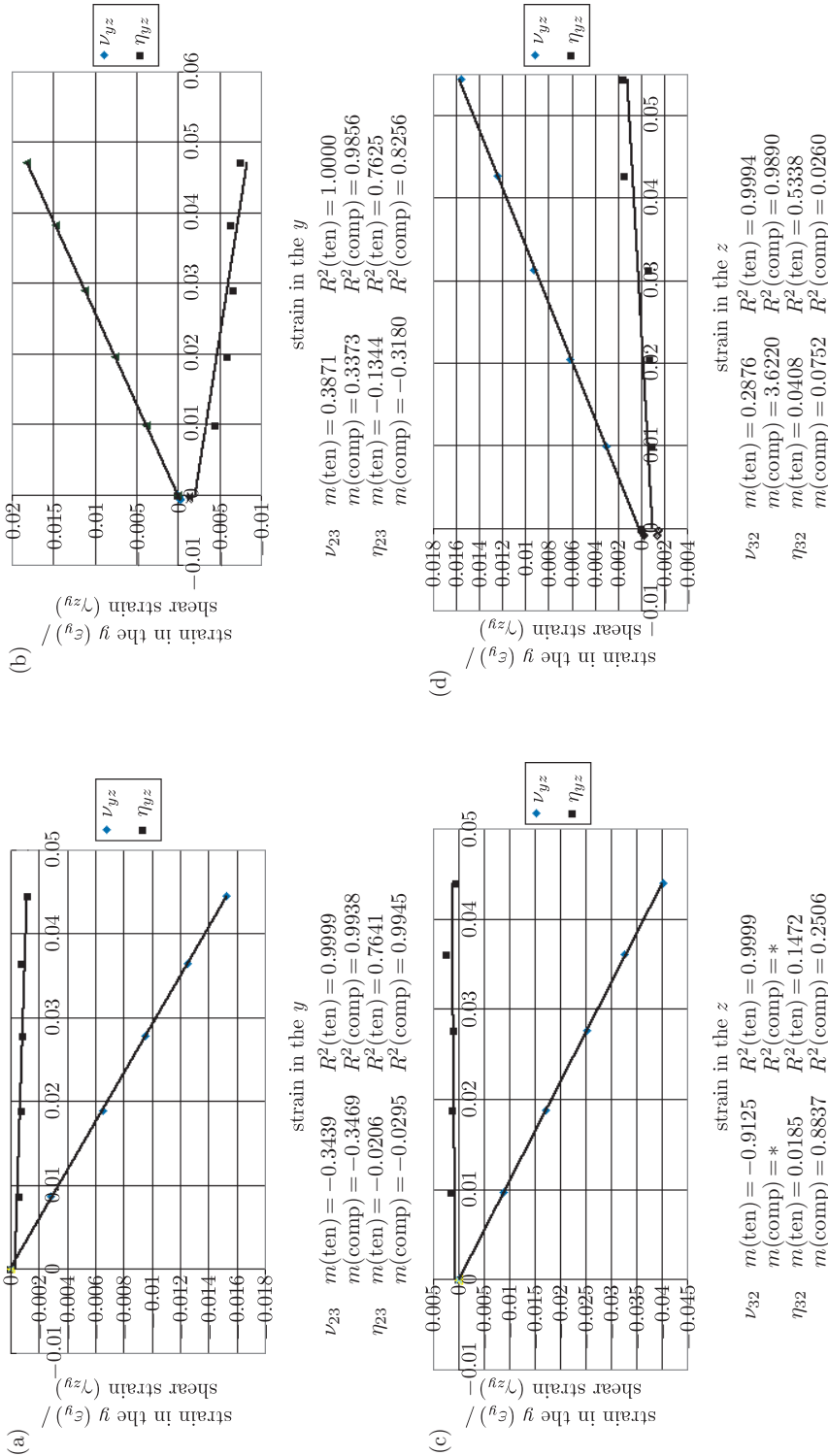


**Figure 5.** The plots obtained for the Poisson's ratios and Coupling coefficients from the strain-strain plots (upon tensile loading) in the Y and Z directions for (1,4)-flexyne (a) & (c) respectively, and for (1,4)-reflexyne (b) & (d) respectively, using the conjugate gradient method, where  $m$  is the gradient of the plot NOTE that \* indicates that the values where not computed



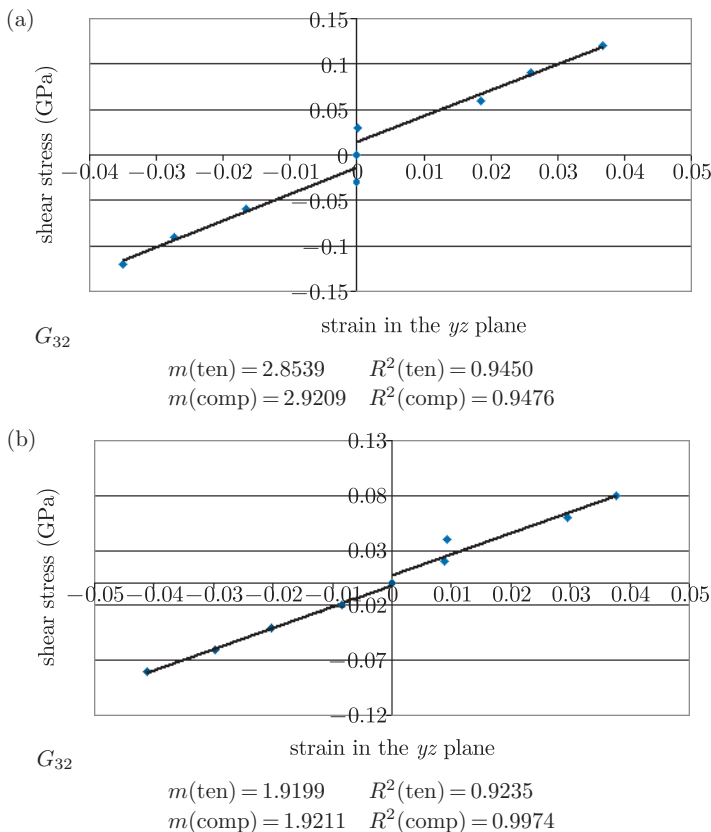


**Figure 6.** The plots obtained for the shear modulus from the shear stress-shear strain plots in the  $ZY$  plane for (1,4)-flexyne (a) and for (1,4)-reflexyne (b) using the conjugate gradient method, where  $m$  is the gradient of the plot

the range of stresses (*i.e.* the initial and final stresses). This information is used for all six sweeps, irrespective of the Young's modulus and shear modulus of the system in the direction of loading.

This procedure can result in problems since:

- when the applied stress is too large, the system may deform past linear “stress and strain”, a problem which could be amplified if the interactions “holding the material together” is of a non-covalent nature;
- when the applied stress is too small, the system will experience very little change (the stresses would be too small to be “felt” by the system) and any differences in the projections recorded can be mainly attributed to the different “minimisation paths”.

In fact, in an ideal scenario, it is desirable the loads used in the simulations are such that they are around 0.5–5% of the moduli<sup>5</sup> in the respective plane. This

5. In some cases, it may be possible to use lower values provided that the stresses are “felt” by the system and a linear relationship is obtained for a stress-strain graph.

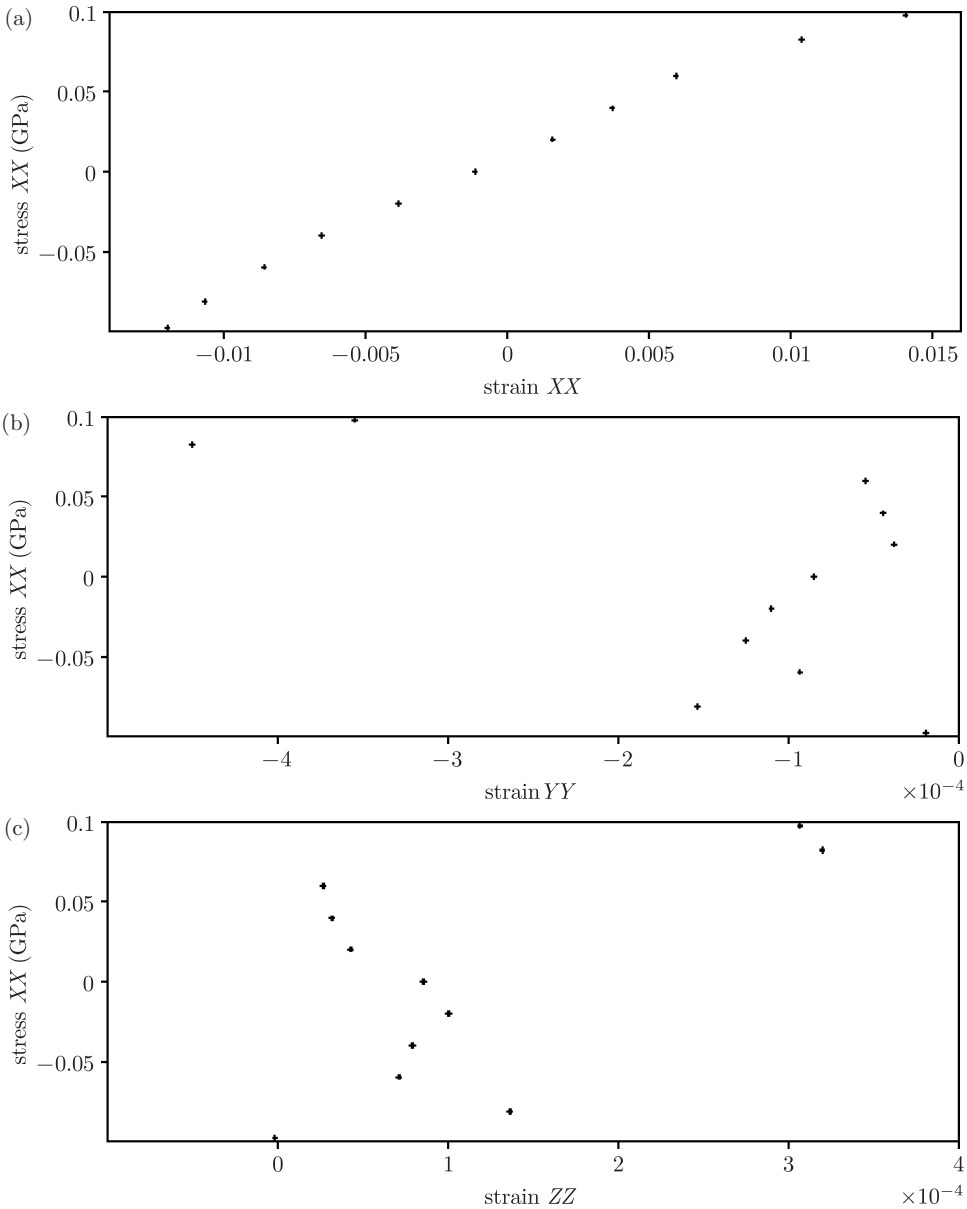


**Figure 7.** Stress–Strain relationships as obtained from *Cerius<sup>2</sup>* automated constant stress method, highlighting the fact that for the plots (b)  $\sigma_x/\varepsilon_y$  (equivalent to  $\nu_{21}$ ) and (c)  $\sigma_x/\varepsilon_z$  (equivalent to  $\nu_{31}$ ) a non-linear relationship is obtained, as opposed to (a)  $\sigma_x/\varepsilon_x$

problem, (*i.e.* that a particular magnitude of stress could be too large for loading in one direction but too small for loading in another direction), can be overcome if the constant strain method is run “manually” by the user (the “manual constant stress method”), since in this case, the user has complete control over each value of stress applied.

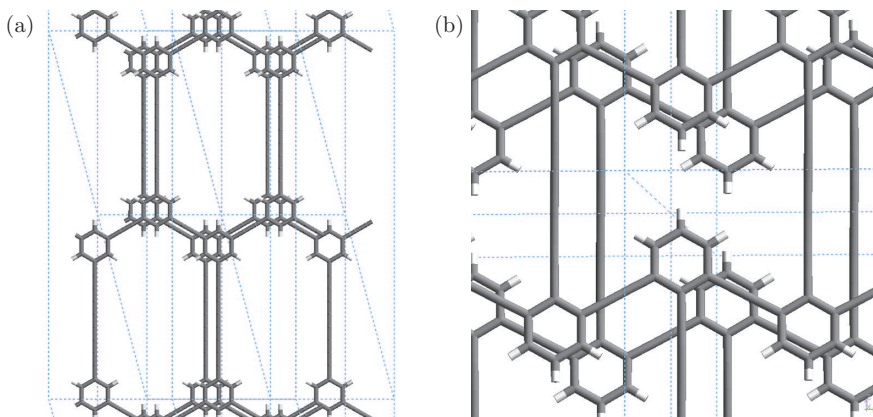


**Figure 8.** The conformation adopted by the phenyl rings in (a) (1,4)-flexyne and (b) (1,4)-reflexyne

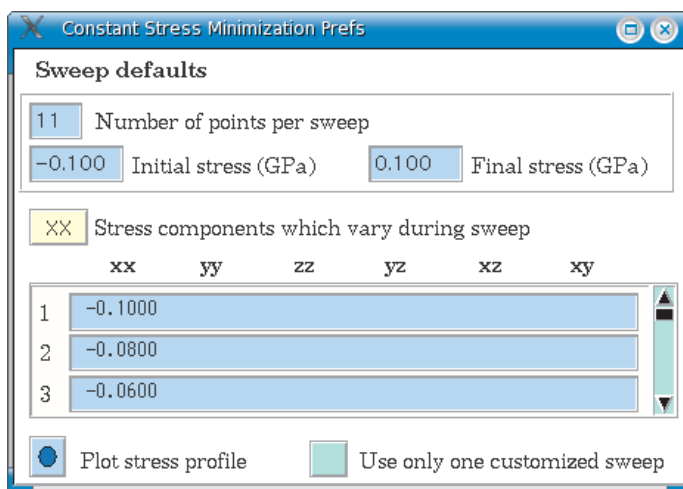


**Figure 9.** The user defined options for the automated constant stress method in *Cerius*<sup>2</sup>.

This complete control over the stresses that can be applied, proved to be a very useful property in the modelling of our systems. This is because at “larger” stresses in compressive on-axis loading (*e.g.* larger than 2% of Young’s modulus), the structure deformed beyond recognition (“imploded”), particularly for loading in the *Z*-direction. This made it necessary to use a different set of stresses for tension than that used in compression. Furthermore, we found that there are significant differences in the results of the mechanical properties if we consider the data “in tension” or “in compression” exclusively. In fact, one may observe that the data obtained by the “automated methods” give an average of the “tension” / “compression” behaviour of these materials.

An explanation for this different behaviour in tension and compression could be due to the fact that in compression in the *Z*-direction at stresses which are

higher than the critical buckling load<sup>6</sup> for the vertical ribs, will result in buckling of these ribs, something which would not occur in tension. Furthermore, it is also possible that this effect is due to the fact that these systems cannot be treated as “simple mechanical systems” since at these scales of structure, the non-bond interactions, which are different in tension and compression, play a significant role in determining the properties of these systems.

Nevertheless, despite the differences identified here, it should be noted that when one considers the fact that:

- irrespective of the method used, the differences in the simulated properties, are within  $\pm 5\%$ , *i. e.* typical of the accuracy normally associated with any force-field based study;
- the time taken for the second derivative method to compute the full set of  $6 \times 6$  elastic constants is significantly lower than that required for any of the other processes;

one may conclude that the second derivative method gives the best results in terms of “quality/time” considerations.

### 3.3. Conclusion

From this section we have found that:

- (1) We can reproduce the published data for (1,4)-flexyne and (1,4)-reflexyne. This is very important as it will ensure that our methodology conforms to that used by other workers. We have confirmed that the re-entrant (1,4)-reflexyne exhibits auxetic behaviour;
- (2) We have identified that ideally, due to the fact that there are differences in the values of the mechanical properties if one only analyses the data “in tension” or only “in compression”, for optimal quality of the simulated results, one should use a manual constant stress method so as to have complete control on the simulation;
- (3) Since the differences between the different methods are within the accuracy expected for force-field based simulations, one may conclude that the second derivative method gives the best results in terms of ‘quality/time’ considerations;
- (4) We have found that these materials have a very practical limitation since they have a very low shear modulus. This makes these materials vulnerable to shear.

---

6. The “critical load” is the maximum load, which causes a “column” to be in a state of unstable equilibrium, that is, any increase in the loads or the introduction of the slightest lateral force will cause the “column” to fail by buckling.

## 4. Simulation of the structure and on-axis mechanical properties of other $(n,m)$ -flexyne and $(n,m)$ -reflexyne using the DREIDING force-field

In the previous section, we have simulated the on-axis properties of (1,4)-flexyne and (1,4)-reflexyne networks using the DREIDING force-field and showed that (1,4)-flexyne and (1,4)-reflexyne exhibit positive and negative on-axis Poisson's ratios respectively. Here we will extend this study in order to study the effect of increasing/decreasing the size of the vertical and/or lateral branches of the flexyne/reflexyne systems. In particular we will simulate the properties of (1,2)-, (1,6)-, (2,2)-, (2,4)- and (2,6)-flexynes and (1,5)-, (1,6)-, (2,5)-, (2,6)- and (2,8)-reflexynes using the DREIDING force-field.

### 4.1. Simulations

The methodology used in this chapter was similar to the one used in previous section (Script 1). The only two differences were that a number of new structures were introduced in line 9, whilst lines 31 to 43 were deleted since only the second derivative method was employed. In this section, the mechanical properties were measured using only the second derivative method since this method was found to give the best quality/time ratio for these organic systems<sup>7</sup>.

### 4.2. Results and Discussion

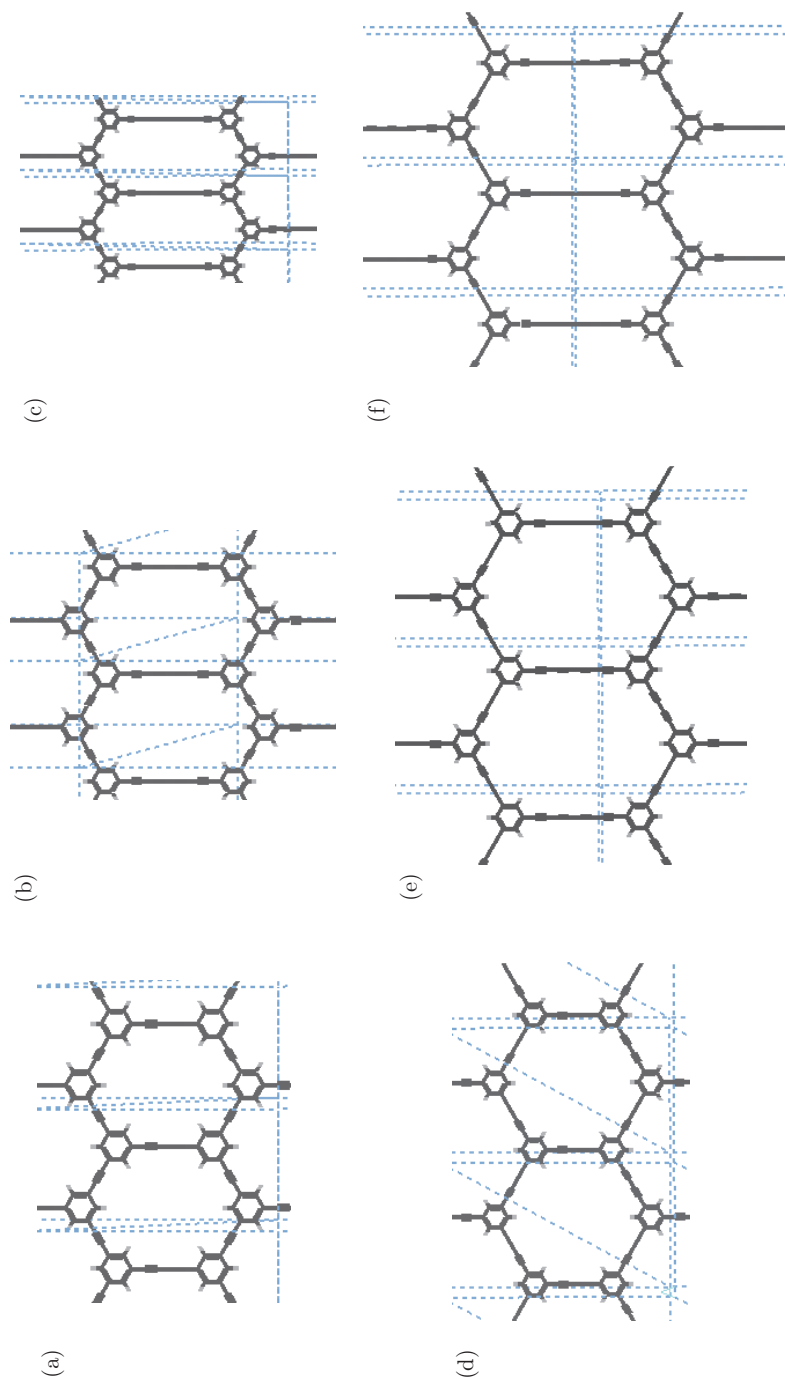
The minimised conformations of  $(n,m)$ -flexyne and  $(n,m)$ -reflexyne are obtained from the DREIDING force-field are shown in Figure 10 and Figure 11 respectively. The on-axis mechanical properties are shown in Table 5 and Table 6 whilst Figure 12 show a comparison of the mechanical properties of  $(n,m)$ -flexyne and  $(n,m)$ -reflexyne.

Table 5 and Table 6 show that our simulated results are comparable with the ones in the literature. This is very significant as it confirms that our methodology is comparable to the one published in the literature. We also attempted to relate the simulated mechanical properties to the geometry of the models.

The projection of the models in the  $YZ$  plane is shown in Figure 10. This shows that for the  $(n,m)$ -flexynes investigated in this study, the use of the DREIDING force-field results in minimum energy structures with "straight" acetylene chains. On the other hand, one may note, as highlighted in Figure 11 that in the case of  $(n,m)$ -reflexynes the vertical chains are not always straight and they tend to start "bending" in the vertical direction as the size of the acetylene links joining the phenyl rings increases. This effect is more evident for  $(2,n)$ -reflexynes than for  $(1,n)$ -reflexynes. Moreover, one may note that unlike the flexynes, the reflexynes are not perfectly planar in the third direction (see Figure 13 (a) and (b)).

---

7. As noted above, there are differences in the results of the mechanical properties if one only analyses the data "in tension" or only "in compression". However, since these differences are not too large, and because of time constraints, the second derivative method was employed.



**Figure 10.** The minimum energy conformations of (a) (1,2)-, (b) (1,4)- (c) (1,-6)-, (d) (2,2)-, (e) (2,4)-, (f) (2,6)-flexyne as obtained using the DREIDING force-field

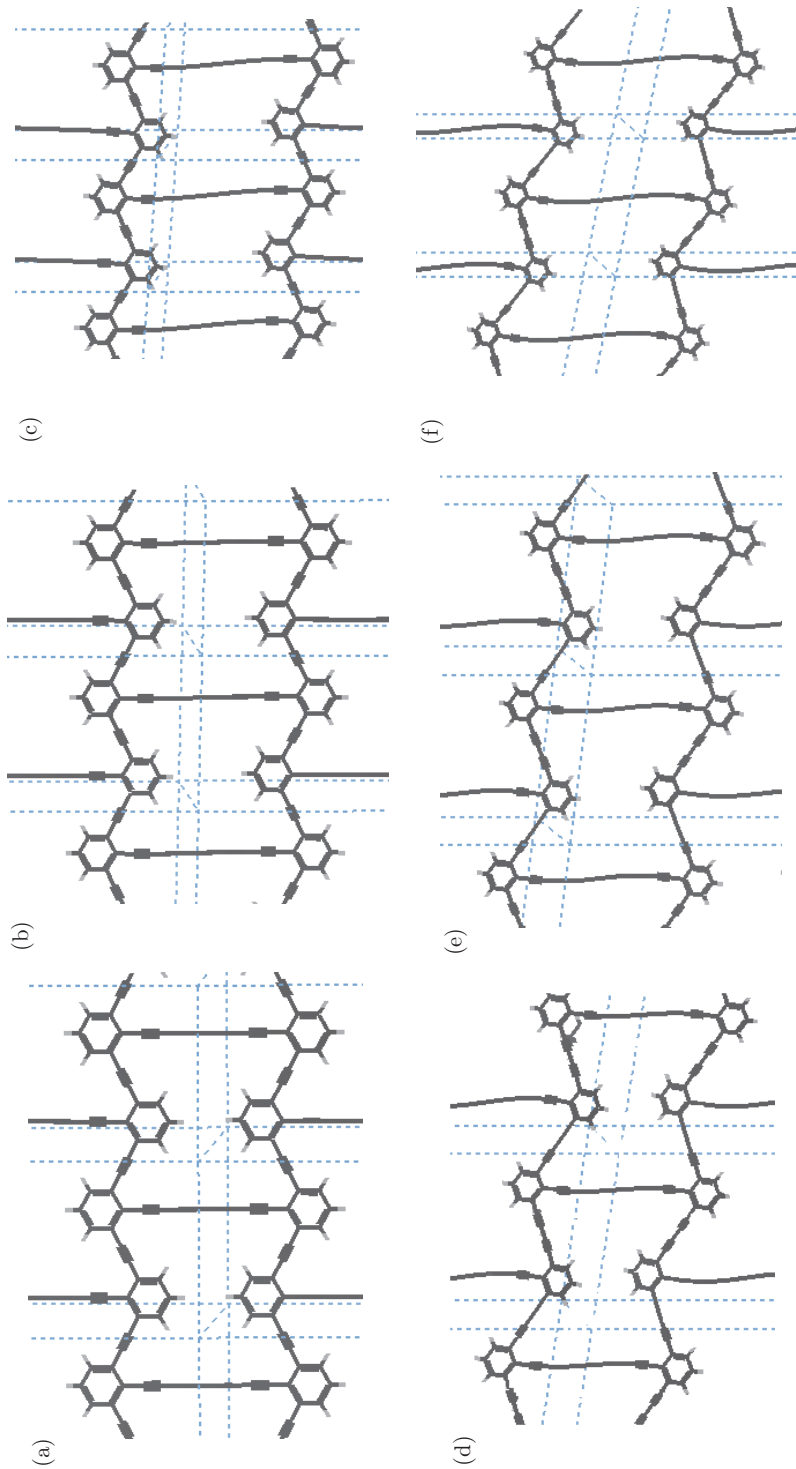


**Figure 11.** The minimum energy conformations of (a) (1,2)-, (b) (1,4)- (c) (1,-6)-, (d) (2,2)-, (e) (2,4)-, (f) (2,6)-reflexyne as obtained using the DREIDING force-field

**Table 5.** The results obtained for  $(n,m)$ -flexyne using the Dredding 2.21 force-field

	Young's moduli (GPa)				Poisson's ratios						Shear moduli (GPa)		
	$E_x$	$E_y$	$E_z$	$\nu_{xy}$	$\nu_{yx}$	$\nu_{xz}$	$\nu_{zx}$	$\nu_{yz}$	$\nu_{zy}$	$G_{xy}$	$G_{yz}$	$G_{xz}$	
(1,2)-flexyne	This study	8.95	77.21	113.17	0.00	0.00	-0.04	0.48	0.03	0.70	0.22	12.08	
	Evans	N//A	75	120	N//A	N//A	N//A	0.46	N//A	0.696	N//A	N//A	
	Alderson	N//A	76	111	N//A	N//A	N//A	0.48	N//A	0.698	N//A	N//A	
(1,4)-flexyne	This study	6.44	55.63	142.98	0.00	0.00	-0.04	0.34	0.04	0.88	0.21	3.31	
	Evans	N//A	56.2	160	N//A	N//A	N//A	0.32	N//A	0.9	N//A	N//A	
	Alderson	N//A	54.6	140	N//A	N//A	N//A	0.34	N//A	0.88	N//A	N//A	
(1,6)-flexyne	This study	5.23	43.52	167.96	-0.01	0.00	-0.05	0.27	0.06	1.04	0.23	1.43	
	Evans	N//A	45	220	N//A	N//A	N//A	0.24	N//A	0.99	N//A	N//A	
	Alderson	N//A	43	164	N//A	N//A	N//A	0.27	N//A	1.03	N//A	N//A	
(2,2)-flexyne	This study	6.13	29.00	29.02	0.00	0.00	-0.01	0.85	0.00	0.85	0.03	7.94	
	Evans	N//A	30	30	N//A	N//A	N//A	0.85	N//A	0.84	N//A	N//A	
	Alderson	N//A	29	29	N//A	N//A	N//A	0.85	N//A	0.85	N//A	N//A	
(2,4)-flexyne	This study	4.33	21.52	38.25	0.00	0.00	-0.01	0.63	-0.01	1.12	0.08	2.36	
	Evans	N//A	23	42	N//A	N//A	N//A	0.60	N//A	1.11	N//A	N//A	
	Alderson	N//A	22	38	N//A	N//A	N//A	0.63	N//A	1.11	N//A	N//A	
(2,6)-flexyne	This study	3.30	17.13	46.94	0.00	0.00	-0.01	0.50	-0.02	1.36	0.09	1.04	
	Evans	N//A	19	55	N//A	N//A	N//A	0.47	N//A	1.33	N//A	N//A	
	Alderson	N//A	17	47	N//A	N//A	N//A	0.5	N//A	1.36	N//A	N//A	



Table 6. The results obtained for  $(n,m)$ -reflexyne using the Dreiding 2.21 force-field

	Young's moduli (GPa)			Poisson's ratios							Shear moduli (GPa)		
	$E_x$	$E_y$	$E_z$	$\nu_{xy}$	$\nu_{yx}$	$\nu_{zx}$	$\nu_{xz}$	$\nu_{yz}$	$\nu_{zy}$	$G_{xy}$	$G_{yz}$	$G_{xz}$	
(1,4)-reflexyne	This study	10.01	129.69	101.40	0.02	-0.01	0.28	-0.38	-0.08	-0.29	0.65	1.92	0.35
	Evans	N//A	124	110	N//A	N//A	N//A	-0.29	N//A	-0.29	N//A	N//A	N//A
	Alderson	N//A	N//A	N//A	N//A	N//A	N//A	N//A	N//A	N//A	N//A	N//A	N//A
(1,5)-reflexyne	This study	3.23	98.83	105.12	0.00	-0.04	0.08	-0.32	-1.23	-0.34	0.54	1.15	0.15
	Evans	N//A	95	116	N//A	N//A	N//A	-0.29	N//A	-0.386	N//A	N//A	N//A
	Alderson	N//A	94	110	N//A	N//A	N//A	-0.33	N//A	-0.39	N//A	N//A	N//A
(1,6)-reflexyne	This study	7.55	72.57	104.87	0.07	-0.04	0.71	-0.17	-0.57	-0.25	1.75	1.84	1.25
	Evans	N//A	84	140	N//A	N//A	N//A	-0.22	N//A	-0.42	N//A	N//A	N//A
	Alderson	N//A	80	124	N//A	N//A	N//A	-0.28	N//A	-0.44	N//A	N//A	N//A
(2,5)-reflexyne	This study	6.06	43.29	40.40	0.14	0.01	0.97	-0.27	0.05	-0.26	1.63	2.44	0.42
	Evans	N//A	57.4	21	N//A	N//A	N//A	-0.69	N//A	-0.53	N//A	N//A	N//A
	Alderson	N//A	N//A	N//A	N//A	N//A	N//A	N//A	N//A	N//A	N//A	N//A	N//A
(2,6)-reflexyne	This study	4.09	45.29	29.96	0.07	-0.12	0.76	-0.41	-0.86	-0.27	1.25	1.31	0.09
	Evans	N//A	35.8	31	N//A	N//A	N//A	-0.72	N//A	-0.7	N//A	N//A	N//A
	Alderson	N//A	37.2	31	N//A	N//A	N//A	-0.83	N//A	-0.69	N//A	N//A	N//A
(2,8)-reflexyne	This study	3.76	28.05	30.22	0.13	-0.11	0.99	-0.27	-0.87	-0.29	1.24	1.04	0.05
	Evans	N//A	31.4	40	N//A	N//A	N//A	-0.5	N//A	-0.902	N//A	N//A	N//A
	Alderson	N//A	27.9	39	N//A	N//A	N//A	-0.57	N//A	-0.887	N//A	N//A	N//A

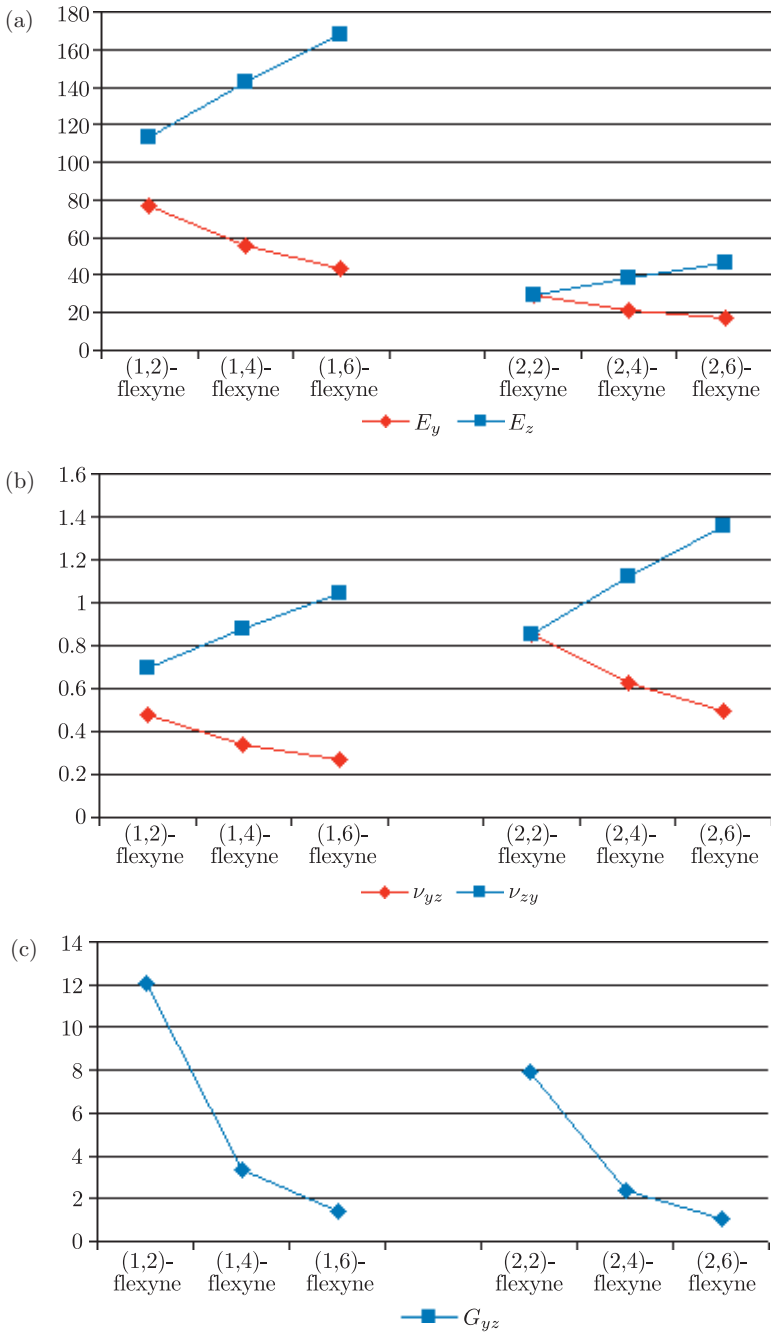
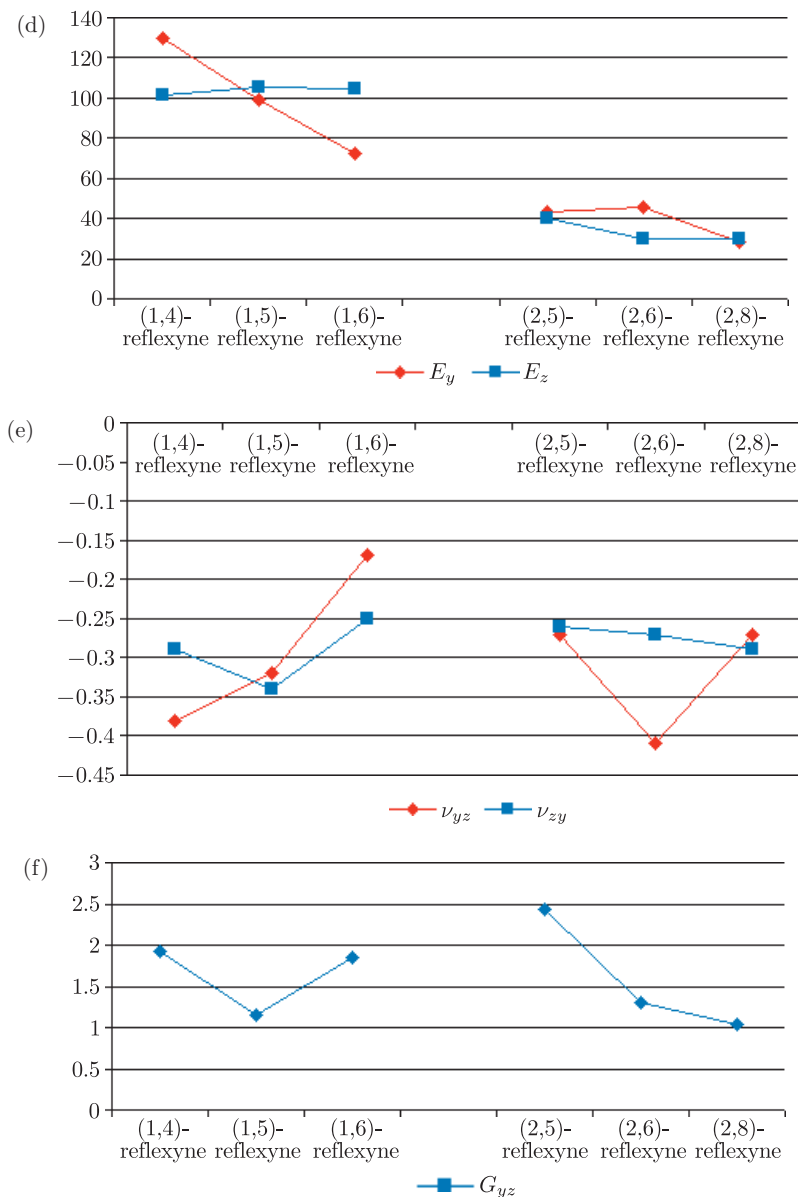


Figure 12. Plots representing the “trends” obtained in the moduli and Poisson’s ratios when comparing the different (n,m)-flexyynes



**Figure 12 – continued.** Plots representing the “trends” obtained in the moduli and Poisson’s ratios when comparing the different  $(n,m)$ -reflexynes

All this may be explained through the fact that, referring to Figure 13, phenyl rings B and E are much closer to each other in the reflexynes when compared to the flexynes. In fact, in the reflexynes the phenyl rings seem to be interacting, perhaps attempting to overlap on each other so as to maximise the  $\pi$ - $\pi$  interactions. The extent of these interactions is dependent on the size of the acetylene bonds as follows:

- If the size of the diagonal acetylene chains is increased, phenyl rings B and E will move towards each other, thus increasing this interaction;
- If the size of the vertical acetylene chains is increased, phenyl rings B and E will move away from each other, thus decreasing this phenyl-phenyl interaction. However, the longer the acetylene chain is, the more flexible it becomes which in turn, results in bending of the chains.

This is not the case in the flexynes, since increasing the diagonal or vertical acetylene chain size results in phenyl rings B and E moving away from each other, maintaining the planar shape of the systems.

The “ease of bending” of the acetylene chains may also be explained from a mechanical point of view in terms of the shear modulus in the  $YZ$  plane which is found to decrease when the size of either the vertical or diagonal acetylene branches is increased, indicating that the structure under study will be more prone to a change in shape. This decrease in the shear modulus upon increasing the size of the acetylene chains is probably primarily due to a decrease in the density of the whole system.

When comparing the mechanical properties of different  $(n,m)$ -flexynes, it is clear that:

- All systems exhibit positive Poisson’s ratios
- Clear trends can be identified to describe the variation of the mechanical properties with the size of the acetylene chains and:
  - In the case of the Young’s moduli there is a clear increase in the  $Z$ -direction and a decrease in the  $Y$ -direction *i.e.* as the size of the acetylene chains increases both in the vertical and diagonal branches, the system will become “harder” in the vertical direction but “softer” in the horizontal direction;
  - In the case of the Poisson’s ratios, although the systems always retain a positive value, when the size of the vertical and/or diagonal acetylene branches is increased, the Poisson’s ratio will become more positive for loading in the  $Z$ -direction but less positive for loading in the  $Y$ -direction;
  - The shear modulus decreases as the size of the acetylene chains increases both in the vertical and diagonal branches

Similar trends (for the Young’s moduli and Poisson’s ratios) were also found in the published data thus further confirming that our methodology is comparable to the one used by other workers.

The change in Poisson’s ratios may be explained by the different mechanisms which may be acting upon the  $(n,m)$ -flexynes. In fact, a conventional honeycomb may deform from either of three mechanisms, namely, hinging, flexing and dilation. For an idealised honeycomb, the former two mechanisms will result in a positive Poisson’s ratio, whilst the latter mechanism results in negative Poisson’s ratios. In organic systems, such the ones being investigated here, one would expect to find these three mechanisms acting concurrently and the Poisson’s ratio would then be expected to depend on the “major” deformation mechanism.

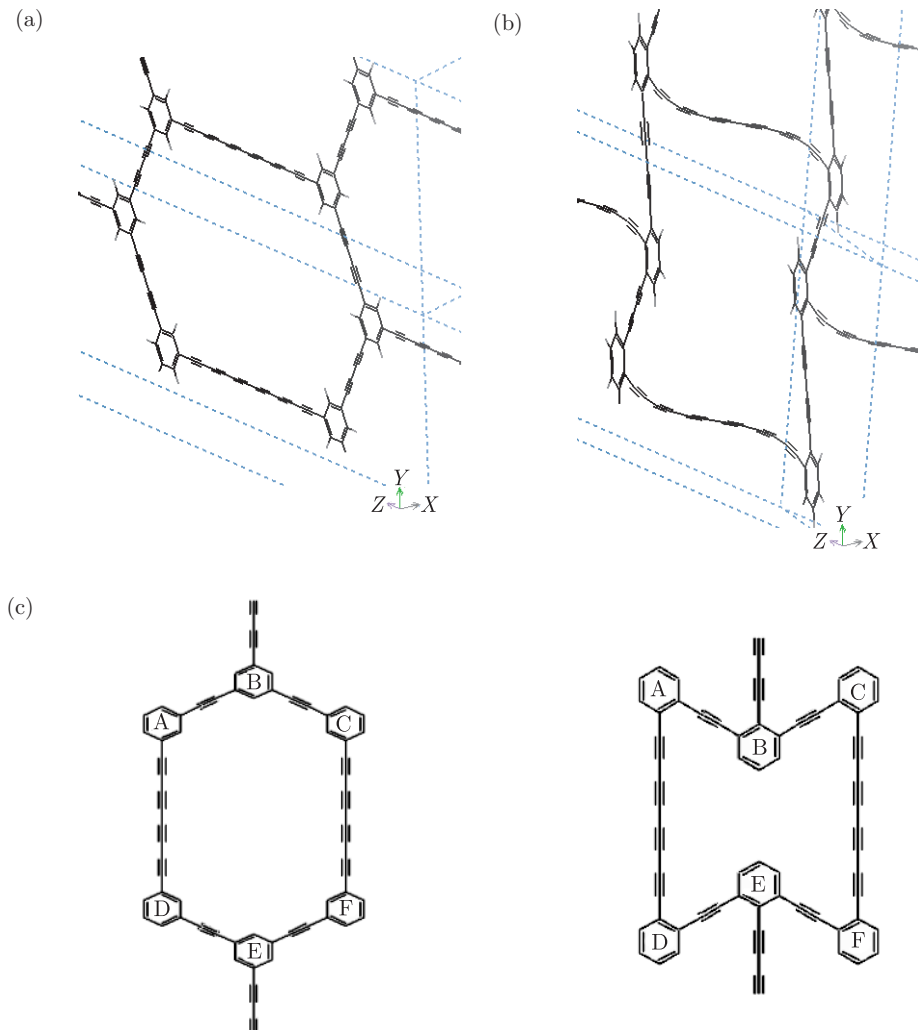


**Figure 13.** The positions of the phenyl rings in the third direction in (a) (2,6)-flexyne and (b) (2,6)-reflexyne. (c) A schematic diagram showing the relative positions of the phenyl rings in flexynes and reflexynes

When considering the  $(n,m)$ -reflexynes systems, it is evident from Figure 12 that:

- All reflexyne systems exhibit negative Poisson's ratios;
- There is no clear trend in the variation of mechanical properties with the length of the acetylene chains can be made was the case for the flexynes.

In fact, the only conclusion that one may draw is that all reflexynes investigated in this study exhibit a negative Poisson's ratio. Similar results (for the Young's moduli and Poisson's ratios) were also found in the published data.

Furthermore, the results confirm that for all systems modelled, the moduli are such that the shear on-axis modulus in the  $YZ$  is extremely low (around 30 times lower than the on-axis Young's moduli). As stated before, this results, which is being reported for the first time, is a very important consideration since it shows that in reality, these materials are expected to be very weak in shear, a property which will reduce the material's suitability for many practical applications. Moreover, the reflexynes always exhibit a lower shear modulus than the flexynes, which as noted above may be explained by the fact that "bending" of the acetylene chains is observed in the reflexynes but not in the flexynes.

It is also interesting to note that when comparing the  $(n,m)$ -flexynes with the  $(n,m)$ -reflexynes one may note that in most cases, the flexynes exhibit a higher in-plane on-axis Young's modulus than the reflexynes. Furthermore, (i) the in-plane on-axis Young's moduli and shear modulus are much higher than the Young's modulus in the third direction or non  $YZ$ -shear moduli, a property which was explained in detail for the (1,4) systems and which apply for all  $(n,m)$  systems.

### 4.3. Conclusion

The results from these simulations clearly suggest that:

- The methodology we are using is comparable to the one used by other workers and published in the literature and the results obtained are very similar;
- As in the case of the published data, for all the flexyne/reflexyne systems modelled, our DREIDING force-field simulations always predict auxetic on-axis behaviour for the reflexynes and conventional on-axis behaviour in the case of the flexynes;
- Clear trends may be identified to describe how the mechanical properties of the flexynes depend on the number of triple bonds in acetylene chains. No such trends could be identified in the case of the reflexynes;
- In all cases, the shear on-axis modulus in the  $YZ$  is extremely low (around 30 times lower than the on-axis Young's moduli). As stated before, this finding, which is being reported for the first time, is a very important consideration since it shows that in reality, these materials are expected to be very weak in shear, a property which will reduce the material's suitability for many practical applications.

## 5. The on-axis mechanical properties of 2D flexyne and reflexyne polyphenylacetylene networks: An investigation on the dependency of the simulated on-axis properties on the force-field used<sup>8</sup>

In the previous sections we showed that we can successfully reproduce the simulations reported in the literature by Evans [22] and Alderson [23]. In view of

---

8. Simulations on reflexynes using the PCFF force-field have already been reported in another publication [24] and are included here only for the sake of completeness.

all this, in this chapter we shall use the same method (albeit slightly modified) in order to re-simulate the properties of (1,4)-flexyne and (1,4)-reflexyne using various force-fields in an attempt to investigate the dependency, if any, of the simulated mechanical properties on the force-field used. Apart from the DREIDING force-field, which was used in the previous chapter, (as part of the validation study), the force-fields which were chosen for this part of the dissertation were the COMPASS [35, 36], CVFF 300 [37], UNIVERSAL [28] and PCFF [38] force-fields. These force-fields were chosen since they are parameterised to deal with organic systems.

This investigation will be carried out on all the flexynes and reflexynes, *i.e.* (1,2)-, (1,4)-, (1,6)-, (2,2)-, (2,4)- and (2,6)-flexynes and (1,4)-, (1,5)-, (1,6)-, (2,5)-, (2,6)- and (2,8)-reflexynes.

### 5.1. Simulations

The methodology used in this chapter was similar to the one employed in the previous chapter, Script 1. The only two differences were that a “for each” loop was introduced between lines 4 and 5 in order to repeat the script for all the force-fields used in this study, whilst lines 31 to 43 were deleted since only the second derivative method was employed.

### 5.2. Results and Discussion

All the simulations were completed successfully and the simulated values of the Young’s moduli, Poisson’s ratios and Shear moduli for (1,4)-flexyne and (1,4)-reflexyne by the various force-fields used in this study are shown in Table 7. The  $(n,m)$ -flexynes and  $(n,m)$ -reflexynes investigated in this study also showed a good correlation to the results<sup>9</sup> published by Evans [22] and Alderson [23], a summary of which is being reported graphically (see Figure 14).

These results clearly indicate that although the actual values of the simulated properties are force-field dependent, the general trends in the results as identified in the previous chapter are force-field independent for a given system. For example, Figure 14 and Figure 15 show that for (1,4)-flexyne and (1,4)-reflexyne the mechanical properties obtained through all force-fields used in this study yield similar results, and similarly for the other systems.

In particular we note that:

- Irrespective of the force-field used, all reflexynes are predicted to exhibit auxetic on-axis behaviour in the  $YZ$  plane whilst all flexynes with all force-fields are predicted to be conventional on-axis in the  $YZ$  plane;
- Irrespective of the force-field used, all the  $(n,m)$ -flexyne and  $(n,m)$ -reflexyne have:
  - $E_x$  is considerably lower than  $E_y$  and  $E_z$ . As stated in the previous chapter, this may be explained in terms of the bonding where in the  $YZ$  plane the flexynes/reflexynes are bonded together through strong covalent bonds while

---

9. These are reported in the Supplementary information in electronic format

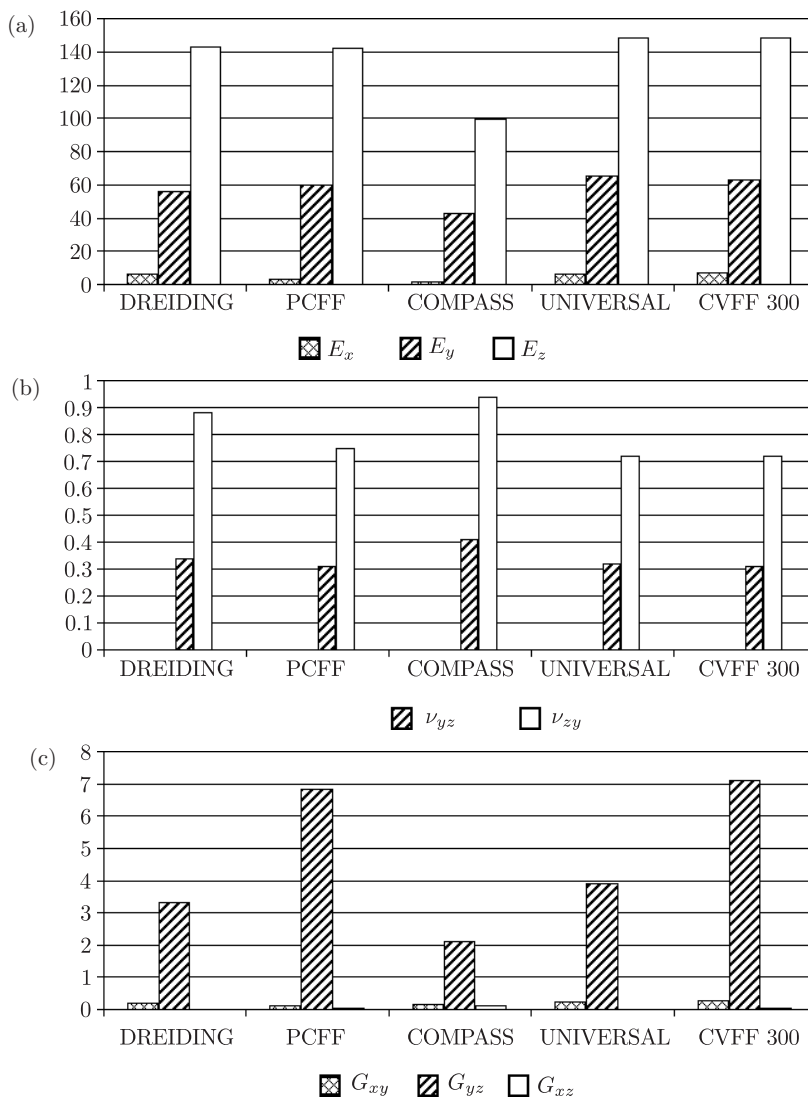
**Table 7.** A table showing the results obtained for (a) (1,4)-reflexyne and (b) (1,4)-flexyne using the different force fields as indicated in the table

		Young's moduli (GPa)					Poisson's ratios					Shear moduli (GPa)				
		$E_x$	$E_y$	$E_z$	$\nu_{xy}$	$\nu_{yz}$	$\nu_{zx}$	$\nu_{yx}$	$\nu_{zy}$	$\nu_{xz}$	$\nu_{xy}$	$\nu_{yz}$	$\nu_{zx}$	$G_{xy}$	$G_{yz}$	$G_{xz}$
Published Data	Evans(1995)	N//A	124	110	N//A	N//A	N//A	N//A	-0.29	N//A	N//A	N//A	N//A	N//A	N//A	N//A
	Alderson(2005)	N//A	N//A	N//A	N//A	N//A	N//A	N//A	N//A	N//A	N//A	N//A	N//A	N//A	N//A	N//A
Force-fields used	DREIDING	10.01	129.69	101.40	0.02	-0.01	0.28	-0.38	-0.08	-0.29	0.65	1.92	0.35			
	PCFF	8.39	120.10	99.43	0.01	0.01	0.16	-0.40	0.15	-0.34	0.32	4.57	0.07			
	COMPASS	7.85	76.75	74.01	0.05	0.00	0.44	-0.54	-0.02	-0.52	0.54	0.70	0.28			
	UNIVERSAL	8.00	137.63	100.63	0.02	-0.01	0.34	-0.44	-0.09	-0.32	0.66	2.45	0.22			
	CVFF 300	9.31	157.24	107.63	0.00	-0.02	0.01	-0.24	-0.26	-0.17	0.90	6.45	0.23			

		Young's moduli (GPa)					Poisson's ratios					Shear moduli (GPa)				
		$E_x$	$E_y$	$E_z$	$\nu_{xy}$	$\nu_{yz}$	$\nu_{zx}$	$\nu_{yx}$	$\nu_{zy}$	$\nu_{xz}$	$\nu_{xy}$	$\nu_{yz}$	$\nu_{zx}$	$G_{xy}$	$G_{yz}$	$G_{xz}$
Published Data	Evans(1995)	N//A	56.2	160	N//A	N//A	N//A	N//A	0.32	N//A	0.9	N//A	N//A	N//A	N//A	
	Alderson(2005)	N//A	54.6	140	N//A	N//A	N//A	N//A	0.34	N//A	0.88	N//A	N//A	N//A	N//A	
Force-fields used	DREIDING	6.44	55.63	142.98	0.00	0.00	-0.04	0.34	0.04	0.88	0.21	3.31	0.01			
	PCFF	2.85	59.44	142.17	0.00	0.00	-0.04	0.31	-0.07	0.75	0.12	6.82	0.04			
	COMPASS	1.59	43.04	99.76	0.00	-0.03	-0.08	0.41	-2.12	0.94	0.16	2.09	0.13			
	UNIVERSAL	6.34	65.55	148.57	0.00	0.00	-0.04	0.32	0.03	0.72	0.22	3.92	0.01			
	CVFF 300	6.83	62.91	148.02	0.00	0.00	-0.03	0.31	-0.09	0.72	0.28	7.09	0.03			





**Figure 14.** Plots showing the absolute values for (a) Young's moduli, (b) Poisson's ratios and (c) shear moduli for (1,4)-flexyne as simulated by different force-fields

in the  $XZ$  and  $XY$  planes they are “loosely” connected together through much weaker non-bond interactions;

- The relative magnitudes of  $E_y : E_z$  remain fairly constant (see Figure 14 and Figure 15 which illustrate this very clearly for (1,4)-flexyne and (1,4)-reflexyne);
- Very low shear moduli in all planes with:
  - (a) A shear modulus very close to zero in the non  $YZ$  plane meaning that there is very little resistance for the layers to slip past each other. As in the case of the Young's moduli, this behaviour may be explained in

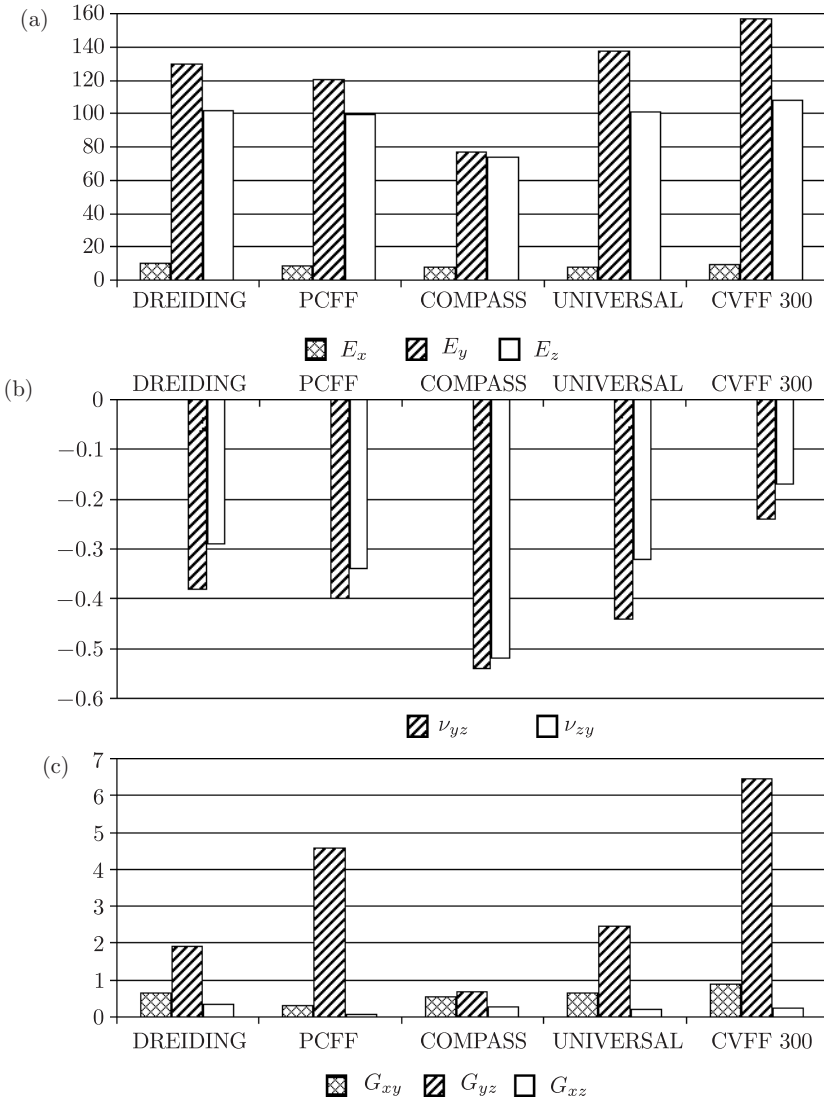


**Figure 15.** Plots showing the absolute values for (a) Young’s moduli, (b) Poisson’s ratios and (c) shear moduli for (1,4)-reflexyne as simulated by different force-fields

terms of the type of bonding present in the different planes *i.e.* the strong covalent bonding in the  $YZ$  plane and the weak non-bond interactions in the  $XY$  and  $XZ$  planes. In fact, one would expect that these graphite-like systems offer no resistance to shearing in the latter two planes as the “infinite” layers making up these system would slide over each other;

- (b) A low (but finite) shear modulus in the  $YZ$  plane (when compared to the on-axis Young’s modulus) indicating that these networks will shear very easily. This is much more pronounced in the reflexynes than in the flexynes.

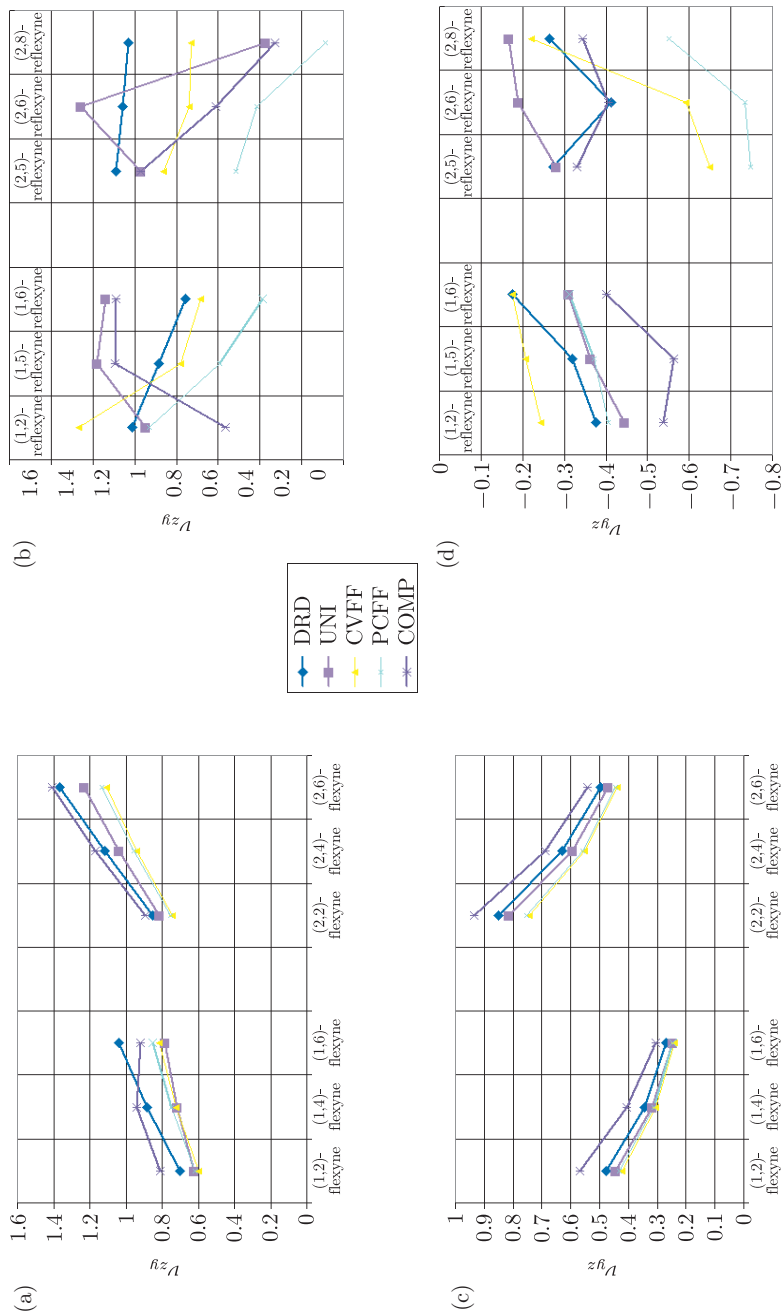


**Figure 16.** Plots showing the absolute values of  $\nu_{xy}$  and  $\nu_{yz}$  for  $(n,m)$ -flexynes (a) & (c) and  $(n,m)$ -reflexynes (b) & (d) as simulated by the different force-fields

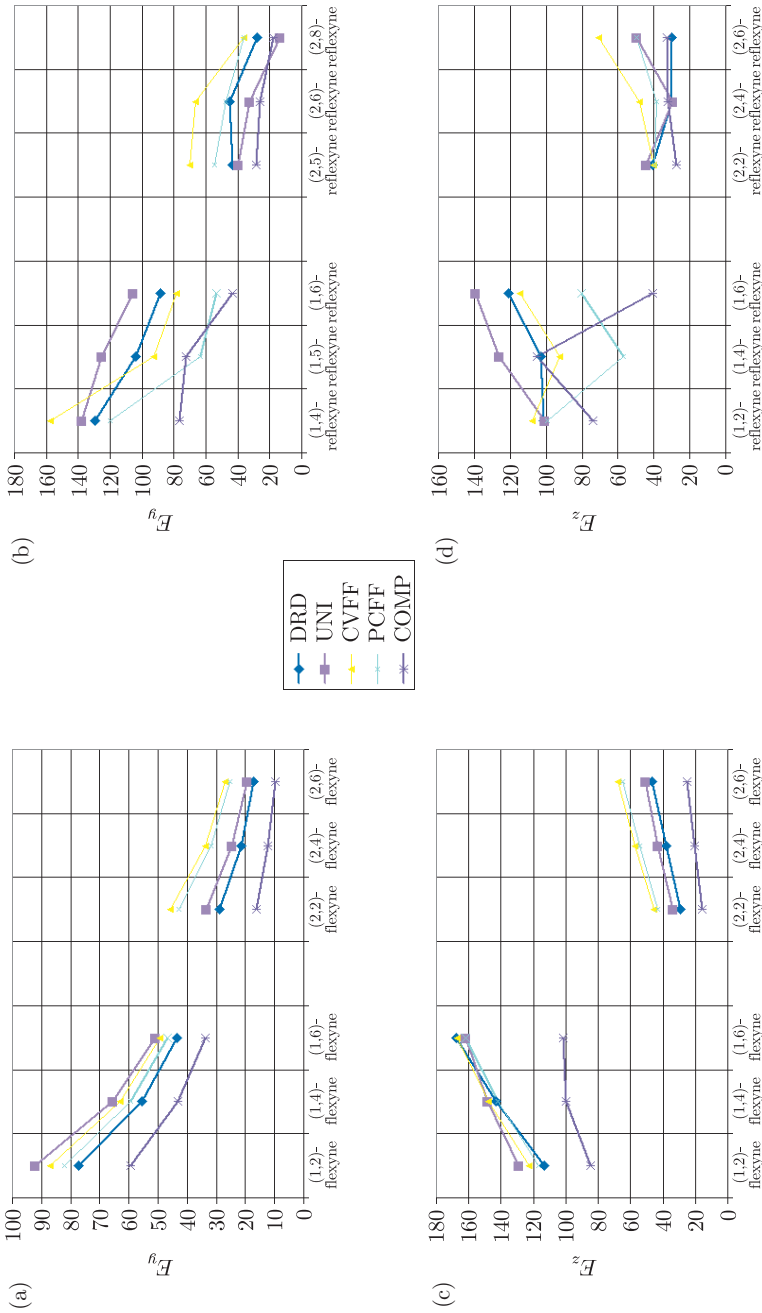


**Figure 17.** Plots showing the absolute values of  $E_y$  and  $E_z$  for  $(n,m)$ -flexynes (a) & (c) and  $(n,m)$ -reflexynes (b) & (d) as simulated by the different force-fields

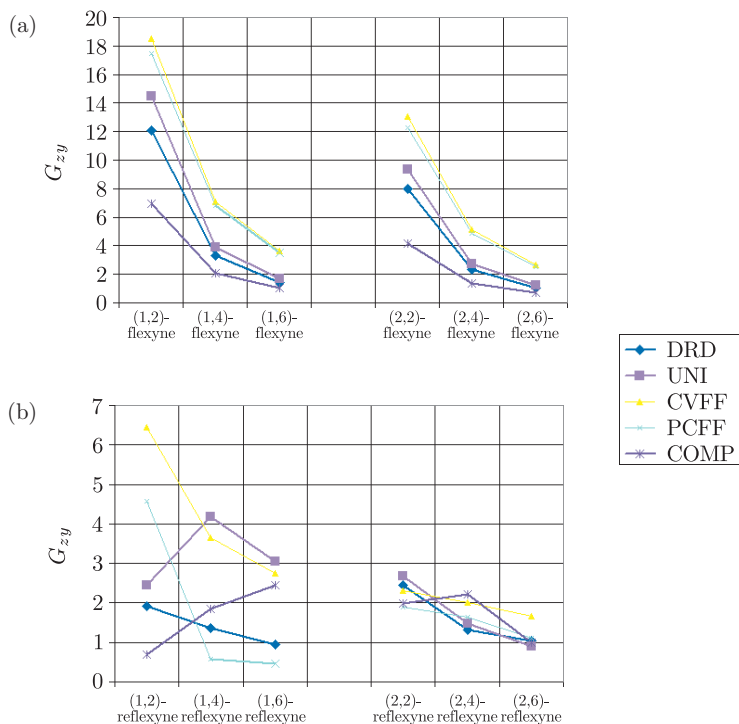


**Figure 18.** Plots showing the absolute values of  $G_{zy}$  ( $n,m$ )-flexynes (a) and ( $n,m$ )-reflexynes (b) as simulated by the different force-fields

- The trends describing the variation of the mechanical properties with the length of the acetylene chains as identified in the previous chapter with the DREIDING force-field remain could also be found with all the other force-fields, *i.e.*:
  - the Young's moduli in the  $Z$ -direction increase whilst those in the  $Y$ -direction decrease;
  - the Poisson's ratios are always positive however, an increase in the size of the vertical and/or diagonal acetylene branches causes the Poisson's ratio to become more positive for loading in the  $Z$ -direction but less positive for loading in the  $Y$ -direction;
  - the in-plane shear modulus decreases as the size of the acetylene chains is increased.

### 5.3. Conclusion

The simulations in this section suggest that despite the fact that the exact magnitudes of the mechanical properties are dependent of the force-field, the general properties of the flexyne and reflexyne systems identified in Chapters 3 and 4 using the DREIDING force-field were not artefacts of the simulations thus adding confidence in the earlier results.

## 6. The off-axis mechanical properties of 2D flexyne and reflexyne polyphenylacetylene networks

In the previous chapter we showed through force-field based simulations that irrespective of the force-field used, reflexyne networks exhibit on-axis negative Poisson's ratios, (*i.e.* auxetic behaviour), the exact magnitude of which depends on the number of triple bonds in the acetylene chains, the force-field used, and even (although to a smaller extent), on the method used to simulate the mechanical properties (*e.g.* manual constant stress vs. second derivative method). It was also very interesting to note that in some cases, the extent of auxeticity was very high, for example in the case of (1,4)-reflexyne, the COMPASS force-field predicted Poisson's ratios  $\nu_{zy} = -0.52$  (The flexyne systems exhibit positive on-axis Poisson's ratios the exact magnitude of which depends on the number of triple bonds in the acetylene chains and the force-field used.)

However, in this investigation (and all other investigations reported in the literature), only the on-axis mechanical properties were measured.

In this section we investigate the off-axis mechanical properties, in particular, the off-axis mechanical properties in the  $YZ$ -plane (the plane of the networks) since no reference has been made to these properties as of yet.

### 6.1. Theory

The standard procedure to obtain the off-axes profiles for mechanical properties for a full rotation around the  $X$ -axis one may make use of the  $6 \times 6$  stiffness matrices  $\mathbf{C} = [c_{mn}]$ , or rather, its parent, the fourth rank stiffness tensor. This  $3 \times 3 \times 3 \times 3$  fourth rank stiffness tensor  $c_{ijkl}$  with stiffness tensorial terms  $c_{ijkl}$  ( $i, j, k, l \in \{1, 2, 3\}$ ) relates to terms  $c_{mn}$  ( $m, n \in \{1, 2, \dots, 6\}$ ), the elements of the  $6 \times 6$  stiffness matrix in such a way that the stiffness tensorial terms  $c_{ijkl}$  ( $i, j, k, l \in \{1, 2, 3\}$ ) may be written in terms of  $c_{mn}$  ( $m, n \in \{1, 2, \dots, 6\}$ ) through replacing pairs of suffixes in  $c_{ijkl}$  by single suffixes according to the following rule:

suffix pair in $c_{ijkl}$ ( <i>i.e.</i> $ij$ or $kl$ )	11	22	33	23,32	31,13	12,21
single suffix in $c_{mn}$	1	2	3	4	5	6

Thus for example,  $c_{11} = c_{1111}$ ,  $c_{14} = c_{1123} = c_{1132}$ ,  $c_{45} = c_{2331} = c_{2313} = c_{3231} = c_{3213}$  and so on.

Having obtained the the fourth rank stiffness tensor  $c_{ijkl}$  describing the mechanical properties in the original orthogonal co-ordinate system  $Ox_{123}$ , this is transformed to  $c_{i'j'k'l'}$  which describes the properties in a new orthogonal co-ordinate system  $Ox'_{123}$ , where  $Ox'_{123}$  is obtained from  $Ox_{123}$  through a simple rotation by an angle  $\zeta'$  around the  $Ox_1$  direction. This transformation is carried out using the tensor transformation rule:

$$c_{i'j'k'l'} = a_{i'i}a_{j'j}a_{k'k}a_{l'l}c_{ijkl} \quad (i, j, k, l, i', j', k', l' \in \{1, 2, 3\}) \quad (8)$$

where  $a_{i'i}$ ,  $a_{j'j}$ ,  $a_{k'k}$  and  $a_{l'l}$  ( $i, j, k, l, i', j', k', l' \in \{1, 2, 3\}$ ) are the elements of the transformation matrix:

$$\begin{pmatrix} 1 & 0 & 0 \\ 0 & \cos(\varsigma) & \sin(\varsigma) \\ 0 & -\sin(\varsigma) & \cos(\varsigma) \end{pmatrix} \tag{9}$$

The “transformed” Poisson’s ratio  $\nu'_{23}$  may be obtained from  $c_{i'j'k'l'}$  by re-obtaining the transformed  $6 \times 6$  stiffness matrix  $\mathbf{C}'$ , inverting it to obtain the transformed  $6 \times 6$  compliance matrix  $\mathbf{S}'$  from which the Poisson’s ratio  $\nu'_{23}$  may be obtained from:

$$\nu'_{23} = -\frac{s'_{32}}{s'_{22}} \tag{10}$$

Alternatively, to avoid the inversion, one may transform the compliance matrix (or rather its parent the 4<sup>th</sup> rank compliance tensor), although in this case, care must be taken as sometimes the transformation the terms of compliance matrix to the terms of the compliance 4<sup>th</sup> rank tensor involve factors of 2 or 4.

However, in our study we are primarily interested a sub-section of the full  $6 \times 6$  stiffness and compliance matrices, namely the  $3 \times 3$  sub-matrix, which relate solely to  $Y$  and  $Z$  directions. These  $3 \times 3$  stiffness and compliance “sub-matrices” relate stress to strain for a 2D system in the  $YZ$  plane and are defined through:

$$\begin{pmatrix} \sigma_y \\ \sigma_z \\ \tau_{yz} \end{pmatrix} = \begin{pmatrix} c_{22} & c_{23} & c_{24} \\ c_{32} & c_{33} & c_{34} \\ c_{42} & c_{43} & c_{44} \end{pmatrix} \begin{pmatrix} \varepsilon_y \\ \varepsilon_z \\ \gamma_{yz} \end{pmatrix} \quad \& \quad \begin{pmatrix} \varepsilon_y \\ \varepsilon_z \\ \gamma_{yz} \end{pmatrix} = \begin{pmatrix} s_{22} & s_{23} & s_{24} \\ s_{32} & s_{33} & s_{34} \\ s_{42} & s_{43} & s_{44} \end{pmatrix} \begin{pmatrix} \sigma_y \\ \sigma_z \\ \tau_{yz} \end{pmatrix}$$

where the terms  $c_{ij}$  and  $s_{ij}$  in the  $3 \times 3$  matrices refer to the respective terms in the original  $6 \times 6$  matrices. In such cases, the parent 4<sup>th</sup> rank tensor is  $2 \times 2 \times 2 \times 2$  and, for example, compliance tensor  $s_{ijkl}$  ( $i, j, k, l \in \{1, 2\}$ ) relate to the sub-matrix  $\mathbf{S}$  above through:

$$\begin{aligned} s_{1111} &= s_{22} & s_{1122} &= s_{23} \\ s_{2211} &= s_{32} & s_{2222} &= s_{33} \\ 2s_{1211} &= 2s_{2111} = s_{42} & 2s_{1222} &= 2s_{2122} = s_{43} \\ \\ 2s_{1112} &= 2s_{1121} = s_{24} \\ 2s_{2212} &= 2s_{2221} = s_{34} \\ 4s_{1212} &= 4s_{1221} = 4s_{2112} = 4s_{2121} = s_{44} \end{aligned}$$

and in this case, the transformation is carried out using the tensor transformation rule:

$$s_{i'j'k'l'} = a_{i'i}a_{j'j}a_{k'k}a_{l'l}s_{ijkl} \quad (i, j, k, l, i', j', k', l' \in \{1, 2\})$$

where  $a_{i'i}$ ,  $a_{j'j}$ ,  $a_{k'k}$  and  $a_{l'l}$  ( $i, j, k, l, i', j', k', l' \in \{1, 2\}$ ) are the elements of the transformation matrix:

$$\begin{pmatrix} \cos(\varsigma) & \sin(\varsigma) \\ -\sin(\varsigma) & \cos(\varsigma) \end{pmatrix}$$

### 6.2. Results and Discussion

The method used to obtain the off-axis plots will be used to transform the  $3 \times 3$  compliance sub-matrix which was calculated through the simulations in the

previous chapters for the various  $(n,m)$ -flexyne and  $(n,m)$ -reflexyne using various force-fields.

In the case on  $(n,m) = (1,4)$  we calculated the off-axis Poisson's ratio and moduli from the compliance data  $(s_{ij})$  simulated and reported in Chapter 3–4<sup>10</sup>. Plots of these properties against  $\zeta$  are given in Table 8 and Table 9.

These plots clearly show some very interesting features namely that:

1. Despite various difference in the actual values of the on-axis properties, the profiles of the off-axis properties (*i.e.* the shapes of the off-axis plots) are virtually identical;
2. The Poisson's ratios are highly dependent on the direction of loading and:
  - (a) In the case of (1,4)-reflexyne, auxeticity is only observed for loading on-axis or in directions very close to it. In fact, these plots suggest that when (1,4)-reflexyne is loaded in the  $YZ$  plane at more than *c.* 10deg on-axis, the in-plane Poisson's ratios becomes positive reaching a maximum positive for loading at *c.* 45deg off-axis. This is very significant as it suggests that if synthesised, (1,4)-reflexyne will only be auxetic for loading in certain very specific directions;
  - (b) In the case of (1,4)-flexyne, the Poisson's ratios will also become more positive reaching a maximum at *c.* 45deg off-axis. However, in this case, the maximum positive Poisson's ratio is always less than the maximum positive Poisson's ratios in (1,4)-reflexyne.
3. The moduli are such that for both (1,4)-flexyne and (1,4)-reflexyne, maximum Young's moduli are exhibited for loading on-axis whilst maximum shear moduli are exhibited for loading at 45deg off-axis.

It was also interesting to note that in the cases when the on-axis data in tension and compression were different, the off-axis plots were such that the tension/compression plots were slightly non-symmetric where “average of these plots” results in a symmetric plot of a shape similar to the plots obtained from data obtained using methods such as the second derivative method. This is very significant as it confirms the conclusion made in Chapters 3 and 4 that the second derivative method offers the best “quality of results : simulation time” ratio, and that in fact, to a first approximation, the data obtained using this method described the behaviour of the material in both tension and compression.

We also simulated the off-axis plots of the other  $(n,m)$ -flexyne/reflexyne systems using the second derivative data obtained in Chapter 3 & 4 and the off-axis Poisson's ratios plots are given in Figure 19 and Figure 20.

These off-axis Poisson's ratios in Figure 19 and Figure 20 show some very interesting features:

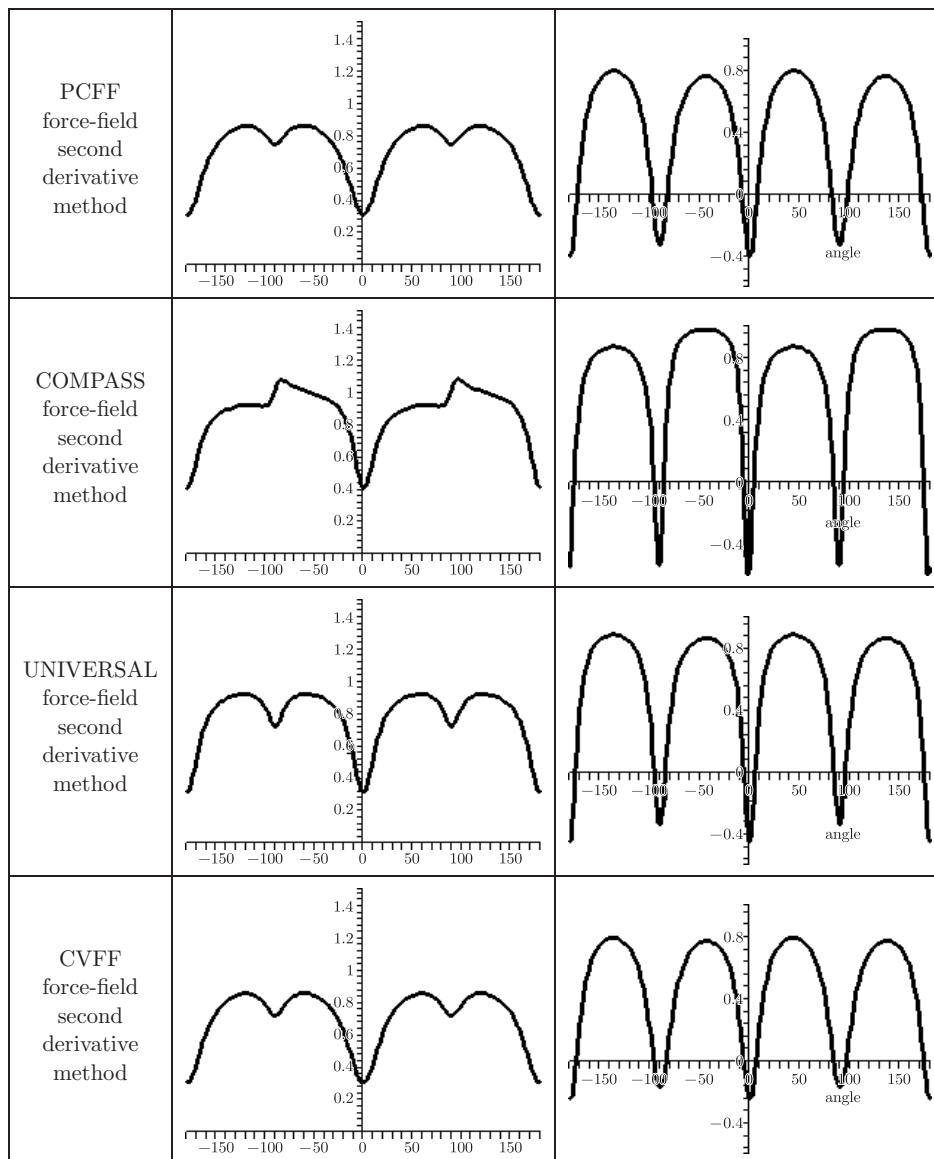
---

10. The data in Chapters 3 and 4 was obtained using the DREIDING force-field through various methods (second derivative, automated constant strain, manual constant stress, *etc.*) whilst the data in Chapter 5 was obtained using various force-fields (CVFF, Universal, PCFF and COMPASS) using the second derivative method.

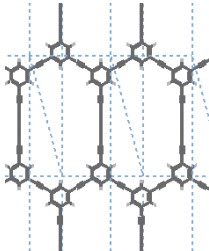
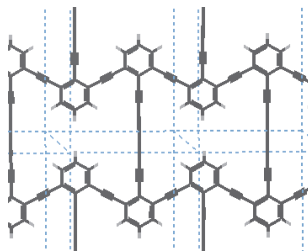
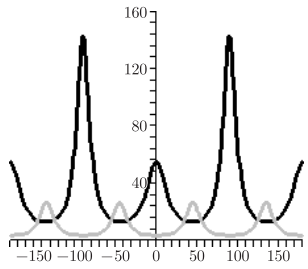
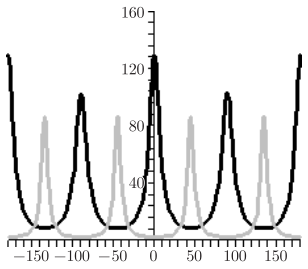
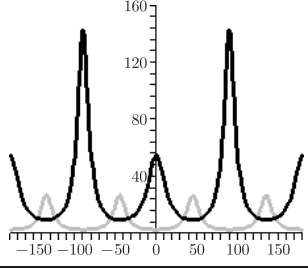
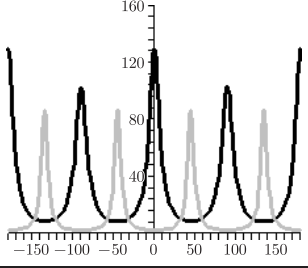
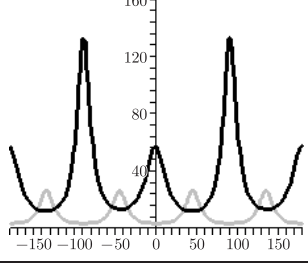
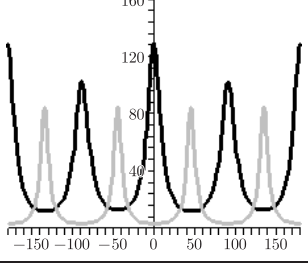
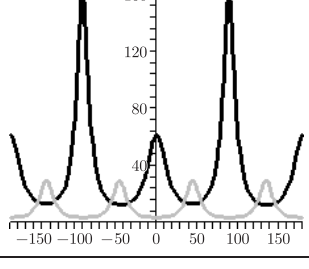
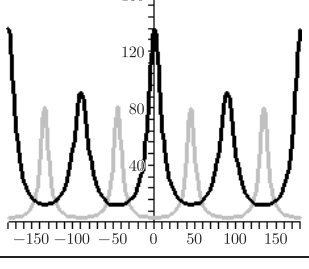


**Table 8.** Plots showing the  $\nu_{yz}$  for (1,4)-flexyne and (1,4)-reflexyne

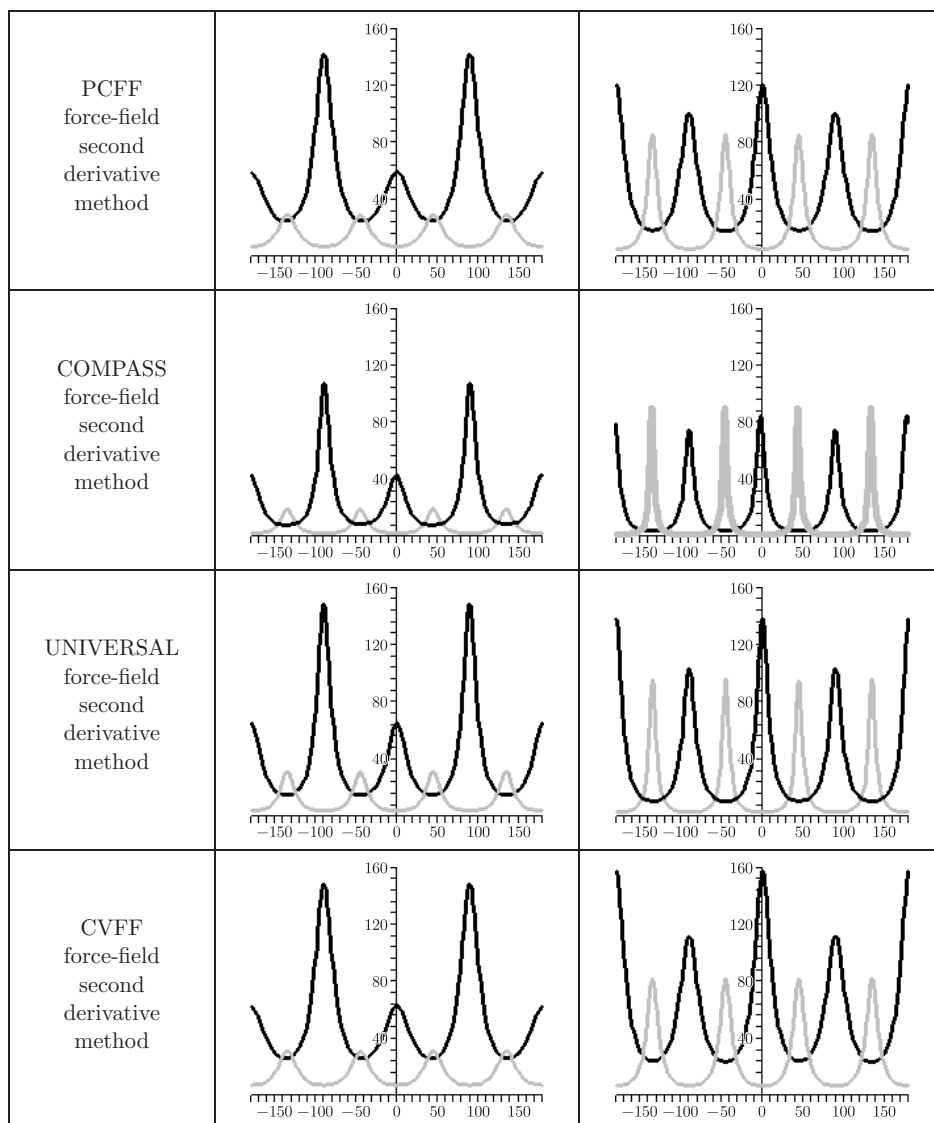
	(1,4)-flexyne $\nu_{yz}$	(1,4)-reflexyne $\nu_{yz}$
Structure		
DREIDING force-field second derivative method		
DREIDING force-field constant strain method		
DREIDING force-field manual constant stress (compression)		
DREIDING force-field manual constant stress (tension)		

Table 8 – continued. Plots showing the  $\nu_{yz}$  for (1,4)-flexyne and (1,4)-reflexyne

**Table 9.** A graph for  $E_y$  (black) and  $G_{zy}$  (gray) for (1,4)-flexyne and (1,4)-reflexyne

	(1,4)-flexyne $\nu_{yz}$	(1,4)-reflexyne $\nu_{yz}$
Structure		
DREIDING force-field second derivative method		
DREIDING force-field constant strain method		
DREIDING force-field manual constant stress (compression)		
DREIDING force-field manual constant stress (tension)		

**Table 9 – continued.** A graph for  $E_y$  (black) and  $G_{zy}$  (gray) for (1,4)-flexyne and (1,4)-reflexyne



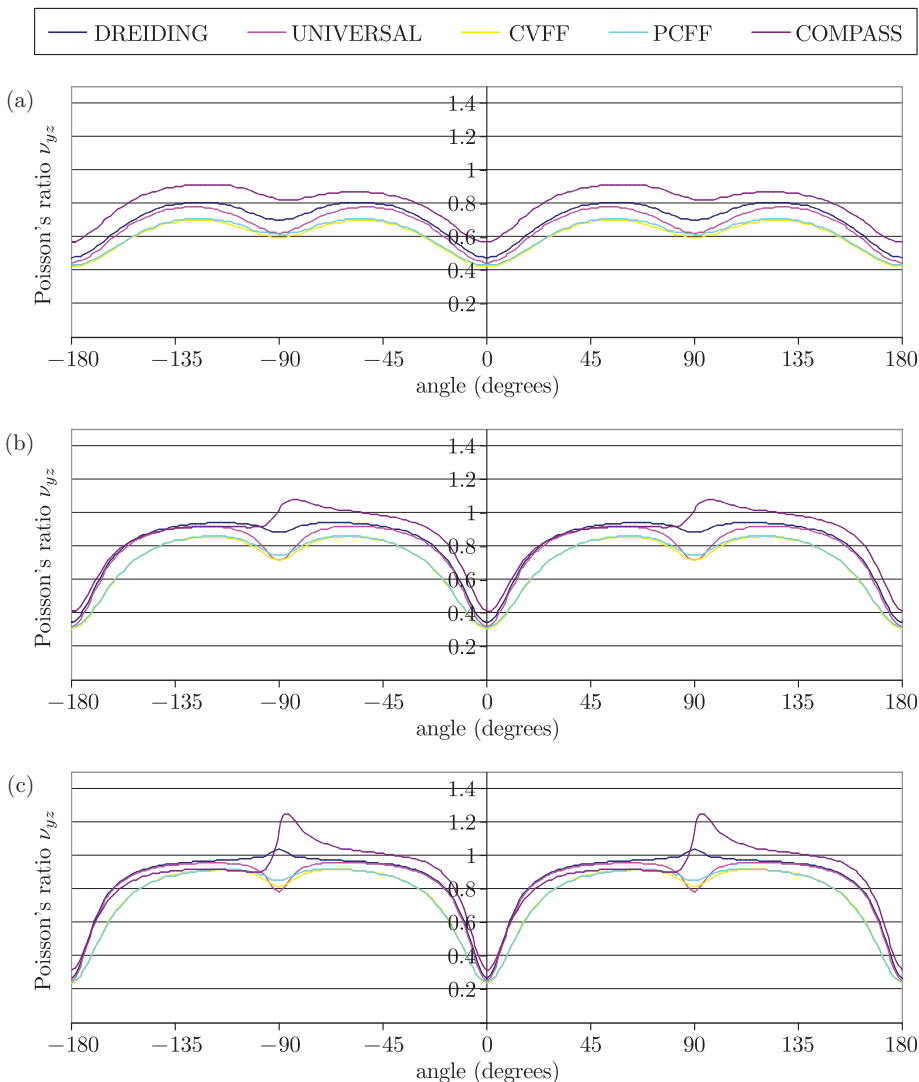


**Figure 19.** Off-axis plots for the  $\nu_{yz}$  (a) (1,2)- (b) (1,4)- (c) (1,6)- flexyne

First (and most significantly), the plots show that the absence of auxeticity in the  $YX$  plane for loading off-axis is a common feature of all the reflexynes. In fact, irrespective of the reflexyne system or force-field used, auxeticity is only exhibited for loading on axis or in directions  $\pm c. 10\text{deg}$  to it. Otherwise, the reflexynes exhibit positive Poisson's ratios, which in most cases approaches  $-1$  when loading at  $c. 45\text{deg}$  off-axis. This is very significant as it clearly shows that the potential of these systems as auxetics for use in practical applications is very limited.

The plots also show that (2,2)-flexyne exhibits (nearly) in-plane isotropy, *i.e.* the Poisson's ratio is independent of the direction of loading. This prop-

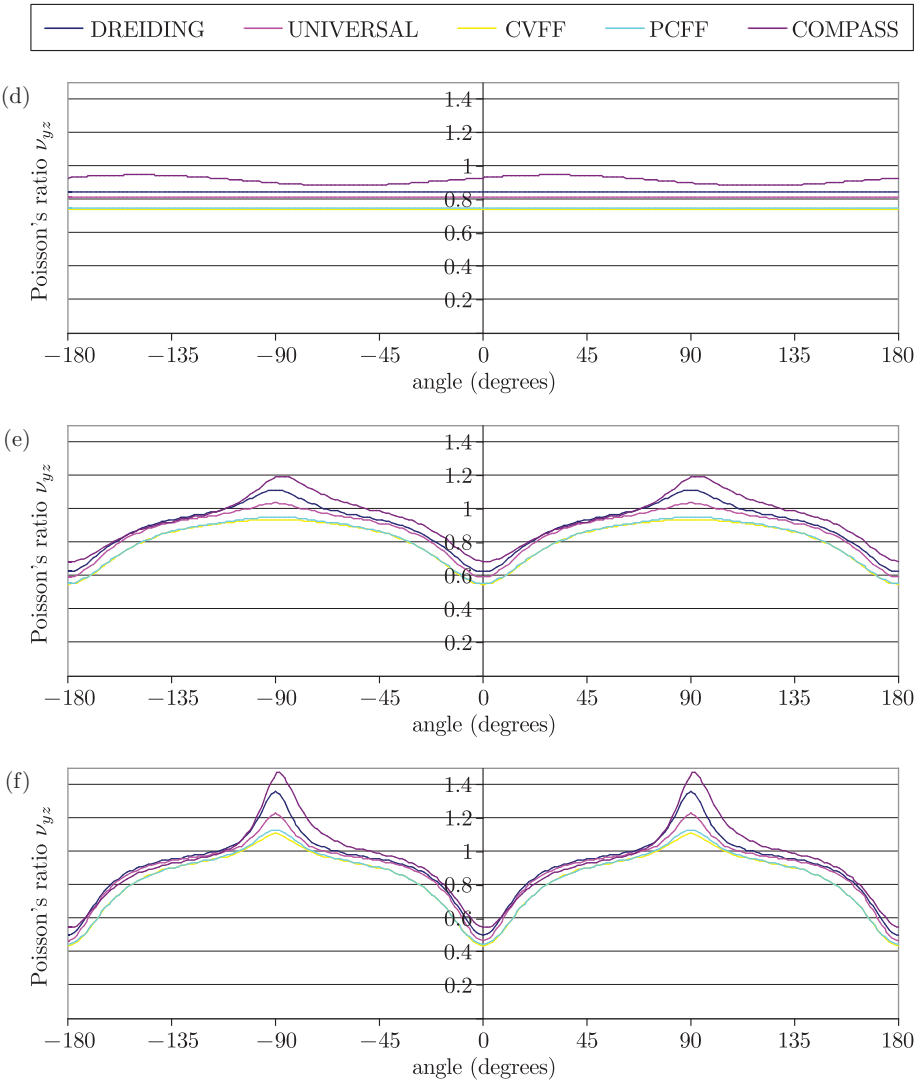


**Figure 19 – continued.** Off-axis plots for the  $\nu_{yz}$  (d) (2,2)- (e) (2,4)- (f) (2,6)- flexyne

erty is the direct result of the symmetry of (2,2)-flexyne (hexagonal). Regrettably, the Poisson's ratio of this system is positive, as expected. The other flexynes exhibit positive in-plane Poisson's ratios for loading in any direction in plane.

### 6.3. Conclusions

The in-plane properties of the flexyne and reflexyne systems are very dependent on the direction of loading. Most importantly, these calculations show that the predicted in-plane on-axis auxeticity is lost when the reflexynes are loaded off-axis.

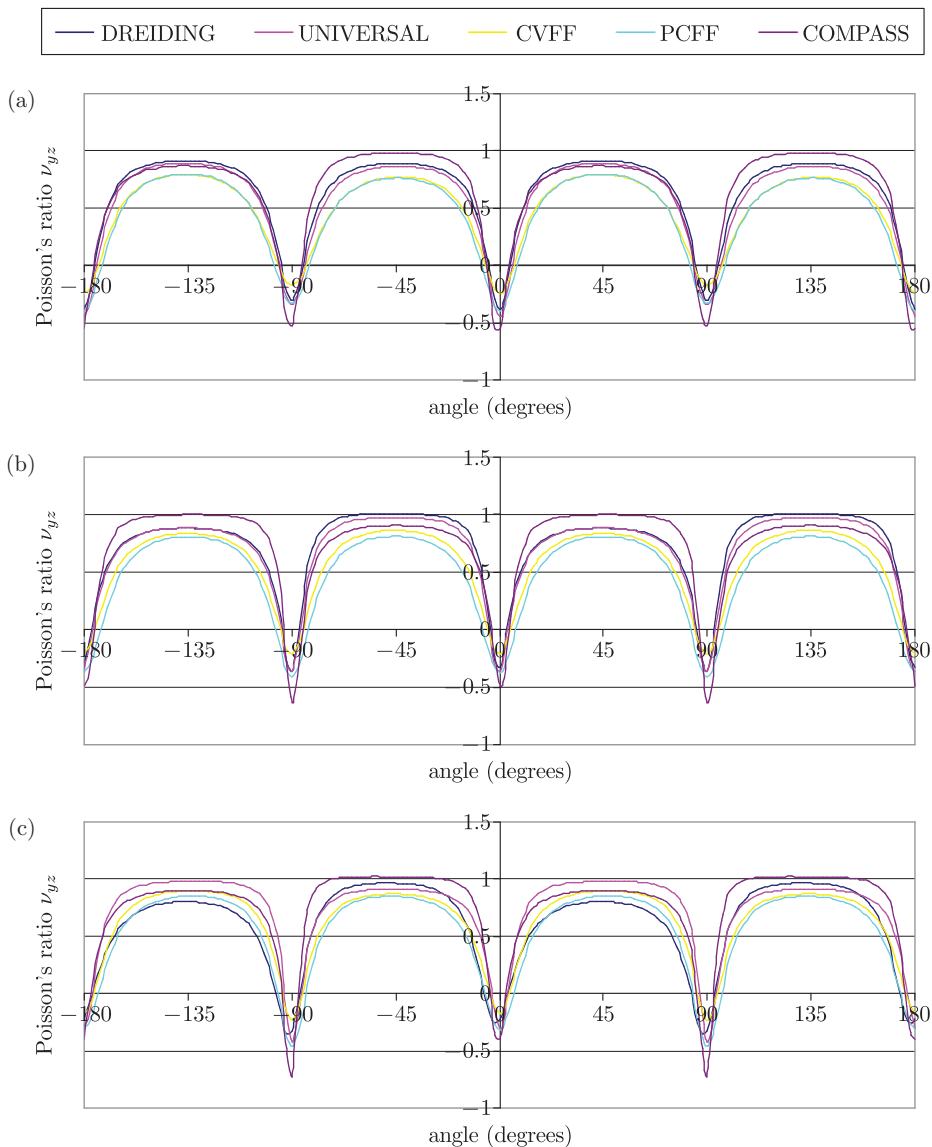


**Figure 20.** Off-axis plots for the  $\nu_{yz}$  (a) (1,4)- (b) (1,5)- (c) (1,6)- reflexyne

## 7. Final Conclusions and Further Research

The main scope of the paper was to make use of empirical modelling techniques in order to derive the full set of mechanical properties of the periodic 2D polyphenylacetylene networks known as flexyne and reflexyne. In particular we attempted to:

- confirm the results obtained from previous studies, which suggested that  $(n,m)$ -flexynes exhibit a positive Poisson's ratio on axis (*i.e.* conventional) whilst  $(n,m)$ -reflexynes exhibit a negative Poisson's ratio on axis (*i.e.* auxetic);

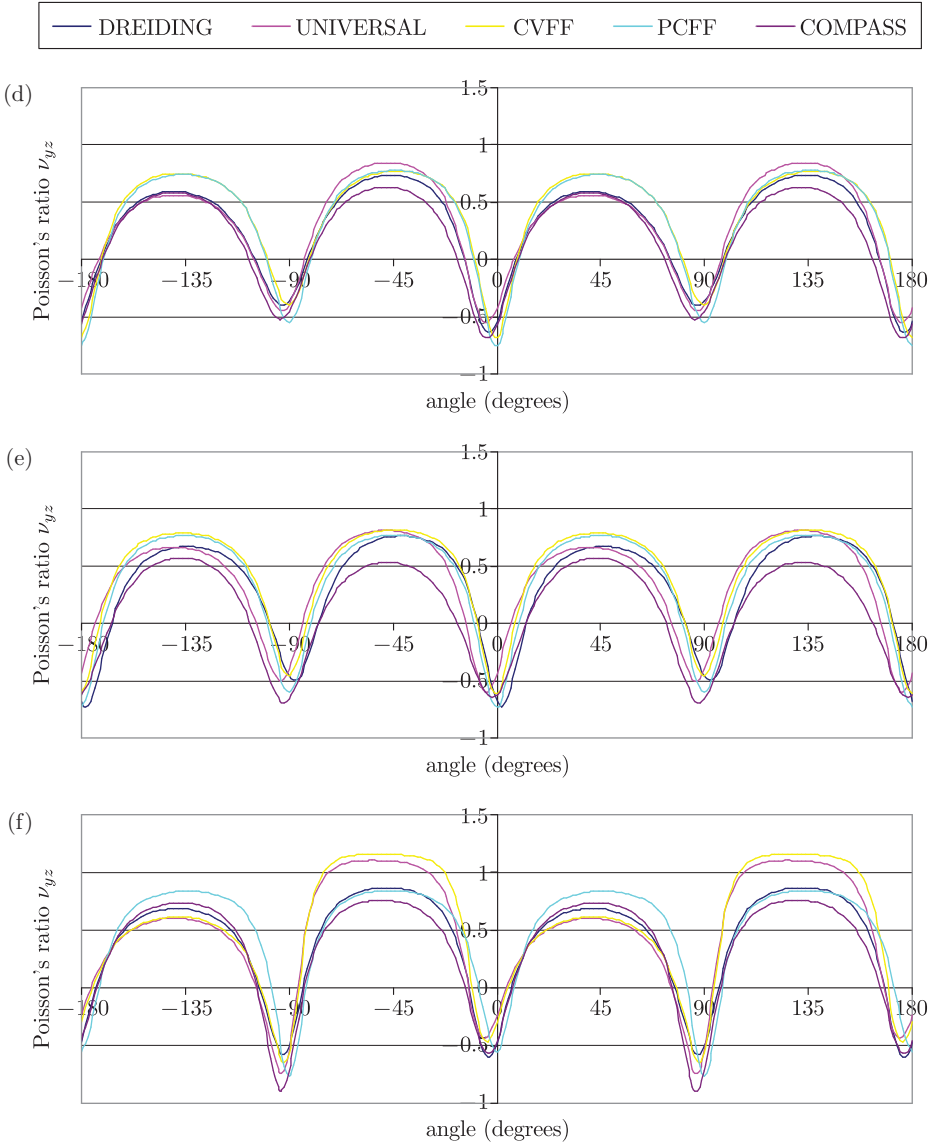


**Figure 20 – continued.** Off-axis plots for the  $\nu_{yz}$  (d) (2,5)- (e) (2,6)- (f) (2,8)- reflexyne

- analyse behaviour of these networks when subjected to shear loads
- analyse the off-axis mechanical properties, particularly the in-plane off-axis Poisson's ratios.

In fact, the first part of the present study was meant to be a validation of our methodology on (1,4)-flexyne and (1,4)-reflexyne and this was accomplished by following a similar methodology employed in the past studies [22, 23] *i.e.* the DREIDING force-field was used. However, our methodology deviated slightly from the other methods with the inclusion of partial charges on each atom (using



Charge Equilibration) and by using various suitable methods for calculating the mechanical properties. From the results obtained, which were similar to the published results, we concluded that in accordance with previous results, the re-entrant (1,4)-reflexyne 2D polyphenylacetylene network is indeed auxetic on-axis whilst (1,4)-flexyne was conventional. We also found that the magnitudes of the simulated on-axis Young's moduli and Poisson's ratios were comparable to those published in the literature. However, we also identified small differences in the actual values of the mechanical properties which were found to be dependent on the method used, and more importantly, dependent on whether the system was analysed in "tension" or in "compression". In view of this, we found that for optimal quality it would be best to use a manual constant stress method rather than an automated one. However, since this method was very time consuming and the differences in the results as obtained from the different methods were relatively low, we further concluded that the "Second Derivative Method" (a method where results were found to be close to the average of the tension/compression data) is the method which gives the best "results:simulation time" ratio. Thus, this method was used in all subsequent studies performed in this dissertation.

We then simulated the properties of other  $(n,m)$ -flexynes/reflexynes using the DREIDING force-field and, in analogy to published work, we identified that all the reflexynes exhibited on-axis auxetic behaviour in the  $YZ$  plane whilst the flexynes exhibited on-axis conventional behaviour. Furthermore, we identified clear trends which describe a relationship between the mechanical properties and the number of triple bonds in acetylene chains for flexynes. No such trends could be identified for the reflexynes, once again, in analogy to previous work. This comparability with previous work was very important not only because it validates our modelling methodology, but also because it ensures that any new data derived for these systems will fit well with the existing published data.

We also found that the Young modulus ( $E_x$ ) is considerably lower than  $E_y$  and  $E_z$ . for all flexynes and reflexynes studied using any force-field. This may be attributed to the fact that the particle interactions are mainly of the non-bond type (*i.e.* weak) in the  $XZ$  and  $XY$  planes while the  $YZ$  plane is dominated by strong covalent bonds.

Finally, we also reported for the first time values for the shear moduli which we have found to be very low (at least an order of magnitude lower than the Young's moduli). This discovery is of great importance as it highlights a very dominant limitation for these materials in practical applications.

We also extended our study to determine whether the results obtained with the DREIDING force-field were force-dependent or independent, a study which is very important when studying novel materials where no experimental data is available for comparison with the simulations. In this study we used the CVFF300, COMPASS, PCFF and UNIVERSAL force-fields, four force-fields which like the DREIDING force-field are adequately parameterised to model systems with phenyl rings and acetylene chains. In this study we found that despite minor differences

in actual values of the simulated mechanical properties when obtained by different force-fields, the general trends identified by the study using the DREIDING force-field were still evident thus suggesting force-field independence of our results. For example, all the force-fields used suggest that reflexynes are auxetic on-axis in the  $YZ$  plane whilst the flexynes are conventional on axis. Another interesting conclusion that we draw regarding the Young's modulus is that for each structure, irrespective of the force-field used, the ratio of the simulated  $E_y: E_z$  appears to remain fairly constant. Low (and sometimes almost negligible) shear moduli were reported using all force-fields. Finally, all force-fields suggest that in the case of the  $(n,m)$ -flexynes the Poisson's ratio become less positive for loading in the  $Y$ -direction upon increasing the size of the vertical/diagonal acetylene branches. This is accompanied by an increase in the Poisson's ratio for loading in the  $Z$ -direction and a decrease in the in-plane shear modulus. The results for the reflexynes did not exhibit a consistent trend and as such no reliable conclusions could be drawn.

The final part of the paper involved a study of the off-axis behaviour of the flexynes and reflexynes. This is "new ground" in the study of these systems since, although numerous publications have emerged on the subject in the last few years, as of yet no reference has been made to these off-axis mechanical properties. From our results we concluded that in general (with the expectation of (2,2)-flexyne which exhibits hexagonal symmetry), the mechanical properties, including the Poisson's ratios are highly dependent on the directions of loading. We found that the Poisson's ratios are always positive in the case of the flexynes, although on axis the Poisson's ratio is at its lowest. In the case of the reflexynes, we found that although all the systems modelled were auxetic in the  $YZ$ -plane on-axis, this auxeticity is lost when loading off-axis. In fact, we found that there are very narrow regions where auxeticity is present. We also found that profiles of the in-plane off axis properties for the same structures were very similar when generated via different force-fields thus once again confirming force-field independence of our simulated results.

All this is once again very significant and of practical importance as it shows that although many reports have been made emphasising the potential of these systems as superior materials in many practical application in view of their auxeticity, (*e.g.* as "smart filters" due to their adjustable pore size on tension and compression), once must now re-examine these claims as such enhanced properties will only be exhibited for loading in very specific directions. All this is in stark contrast to the properties which are exhibited by the polyphenylacetylene-triangles proposed by Grima [39] which are isotropic in plane implying that they can be stretched in any direction in order to bring out their auxetic character. Thus in view of all this the latter would be more appealing in practical applications.

Despite all these "negative" results on the reflexynes, in view of their low shear moduli and off-axis properties, it must be stated that this work has added

more confidence in the claim that “reflexynes are auxetic on-axis” since we have now shown that this result is “independent” of the force-field used in the study.

It is also important to note that this study cannot be treated as the “final” study on these polyphenylacetylene systems. Apart from the fact that from the experimental aspect, much still needs to be done if these systems are to be synthesised and tested, even from the modelling side, despite the many new developments made in this dissertation, there are still many aspects which need to be investigated further.

For example, as regards molecular modelling, there is a lot of room for further investigations particularly since in the case where empirical investigations are carried out the systems are treated as balls and springs – and as a result of this the electrons are ignored. These systems have very interesting electronic properties for example they are expected to exhibit conjugation, hence these polymers have applications as conductive polymers. Such study involving electrons must be performed using a quantum mechanically based approach which are much more computationally intensive.

Additionally, one might consider modelling of a systems made from a finite “sections” of these networks in an attempt to simulate a more realistic system where the sample is not a perfect single crystal. The study can also be extended to newer and better parameterised force-fields as they become available.

Regarding the off-axis properties, another source of further work could be a more detailed investigation in these properties, for example, by studying them in the other planes.

Furthermore, it is important to note that flexynes and reflexynes are not the only polyphenylacetylene networks that can be constructed. The methodology used in this dissertation may also be used (perhaps with some modifications) on other organic networks of a similar nature, such as 3D polyphenylacetylene networks with a (10,3)-*b* topology.

## References

- [1] Evans K E 1991 *Endeavour* **15** 170
- [2] Gliick J 1987 *The New York Times*
- [3] Milton G 1992 *J. Mech. Phys. Solids* **40** 1105
- [4] Grima J N and Evans K E 2000 *Chem. Comm.*, DOI: 10.1039/b004305m
- [5] Lakes R S 1987 *Science* **235** 1038
- [6] Love A E H 1944 *A Treatise on the Mathematical Theory of Elasticity*, 4<sup>th</sup> ed., Dover, New York
- [7] Lakes R S and Elms K 1993 *J. Comp. Mat* **27** 1193
- [8] Choi J B and Lakes R S 1995 *J. Comp. Mat.* **29** 113
- [9] Chen C P and Lakes R S 1996/7 *J. Eng. Mater. Tech, T. ASME* **118** 285
- [10] Smith C W, Grima J N and Evans K E 2000 *Acta Materiala* **48** 4349
- [11] Grima J N, Alderson A and Evans K E 2005 *J. Phys. Soc. Japan* **74** 1341
- [12] Baughman R H and Galvão D S 1993 *Letters to Nature* **365** 735
- [13] Grima J N, Williams J J and Evans K E 2005 *Chem. Comm.* **32** 4065
- [14] He C B, Liu P W and Griffin A C 1998 *Macromolecules* **31** 3145
- [15] He C B, Liu P W, McMullan A C and Griffin A C 2005 *Phys. Stat. Solb.* **242** 576

- 
- [16] Evans K E 1989 *J. Phys. D: Appl. Phys* **22** 1870
- [17] Alderson K L and Evans K E 1993 *J. Mater. Sci.* **28** 4092
- [18] Alderson K L, Kettle A P and Neale P J, Pickles A P, and Evans K E 1997 *Appl. Acoust.* **50** 23
- [19] Baughman R H, Shacklette J M, Zakhidov A A and Stafstrom S 1998 *Nature* **392** 362
- [20] Grima J N, Jackson R, Alderson A and Evans K E 2000 *Adv. Mater.* **12** 1912
- [21] Evans K E, Nkansah M A, Hutchinson I J and Rogers S C 1991 *Nature* **353** 124
- [22] Evans K E, Alderson A and Christian F R 1995 *J. Chem. Soc. Faraday Trans.* **91** 2671
- [23] Alderson A, Davies P J, Williams M R, Evans K E, Alderson K L and Grima J N 2005 *Molecular Simulations* **31** (13) 889
- [24] Grima J N, Attard D, Cassar R, Farrugia L, Trapani L and Gatt R 2008 *Molecular Simulation* **34** 1149
- [25] Grima J N and Attard D 2011 *Phys. Stat. Sol. b* **248** 111
- [26] Gibson L J, Ashby M F, Schajer G S and Robertson C I 1982 *Proc. R. Soc. Lond. A.* **382** 25
- [27] Masters I J and Evans K E 1996 *Comp. Struct.* **35** 403
- [28] Rappe A K and Goddard III W A 1991 *J. Phys. Chem.* **95** 3358
- [29] Allen M P and Tildesley D J 1987 *Computer Simulation of Liquids*, Clarendon Press, Oxford
- [30] Tosi M P 1964 *Solid State Physics*, Springer, **16**
- [31] Kittel C 1986 *Introduction to Solid State Physics*, Wiley
- [32] Karasawa N and Goddard W A 1989 *J. Phys. Chem.* **93** (21) 730
- [33] Ewald P P 1921 *Ann. Phys.*
- [34] Leach R A 2000 *Molecular Modelling, Principles and Applications*, 2<sup>nd</sup> ed., Longman Ltd, U K
- [35] Sun H 1998 *J. Phys. Chem. B*, Molecular Simulation Inc., **102** (38) 7338
- [36] Sun H, Ren P and Fried J R 1998 *Computational and Theoretical Polymer Science* **8** (229-246)
- [37] Dauber-Osguthorpe P, Roberts V A, Osguthorpe D J, Wolff J, Genest M and Hagler A T 1988 *Proteins Struct. Funct. Genet.* **4** 31
- [38] Molecular Simulations Inc. *San Diego*
- [39] Grima J N 2000 *Ph. D. Thesis*, University of Exeter, United Kingdom